New insights into U(VI) sorption onto montmorillonite from batch sorption and spectroscopic studies at increased ionic strength

Stockmann, M.; Fritsch, K.; Bok, F.; Marques Fernandes, M.; Baeyens, B.; Steudtner, R.; Müller, K.; Nebelung, C.; Brendler, V.; Stumpf, T.; Schmeide, K.;

Originally published:

September 2021

Science of the Total Environment 806(2022), 150653

DOI: https://doi.org/10.1016/j.scitotenv.2021.150653

Perma-Link to Publication Repository of HZDR:

https://www.hzdr.de/publications/Publ-32796

New insights into U(VI) sorption onto montmorillonite from batch sorption and spectroscopic studies at increased ionic strength

M. Stockmann [a,*], K. Fritsch [a,1], F. Bok [a], M. Marques Fernandes [b], B. Baeyens [b], R. Steudtner [a], K. Müller [a], C. Nebelung [a], V. Brendler [a], T. Stumpf [a], K. Schmeide [a,*]

[a] *Helmholtz-Zentrum Dresden-Rossendorf, Institute of Resource Ecology, Bautzner Landstr. 400, 01328 Dresden, Germany*

[b] *Paul Scherrer Institute, Laboratory for Waste Management, 5232 Villigen PSI, Switzerland*

Abstract

The influence of ionic strength up to 3 mol kg^{-1} (background electrolytes NaCl or $CaCl_2$) on U(VI) sorption onto montmorillonite was investigated as function of pH_c in absence and presence of CO_2. A multi-method approach combined batch sorption experiments with spectroscopic methods (time-resolved laser-induced fluorescence spectroscopy (TRLFS) and *in situ* attenuated total reflection Fourier-transform infrared spectroscopy (ATR FT-IR)). In the absence of atmospheric carbonate, U(VI) sorption was nearly 99% above pH_c 6 in both NaCl and $CaCl_2$ and no significant effect of ionic strength was found. At lower pH, cation exchange was strongly reduced with increasing ionic strength. In the presence of carbonate, U(VI) sorption was reduced above pH_c 7.5 in NaCl and pH_c 6 in $CaCl_2$ system due to formation of aqueous $UO_2(CO_3)_x^{(2-2x)}$ and $Ca_2UO_2(CO_3)_3$ complexes, respectively, as verified by TRLFS. A significant ionic strength effect was observed due to the formation of $Ca_2UO_2(CO_3)_{3(aq)}$, which strongly decreases U(VI) sorption with increasing ionic strength.

The joint analysis of determined sorption data together with literature data (giving a total of 213 experimental data points) allowed to derive a consistent set of surface complexation reactions and constants based on the 2SPNE SC/CE approach, yielding $\log K^0_{\equiv S^S OUO_2^+} = 2.42 \pm 0.04$, $\log K^0_{\equiv S^S OUO_2OH} = -4.49 \pm 0.7$, and $\log K^0_{\equiv S^S OUO_2(OH)_3^{2-}} = -20.5 \pm 0.4$. Ternary uranyl carbonate surface complexes were not required to describe the data. With this reduced set of surface complexes, an improved robust sorption model was obtained covering a broad variety of geochemical settings over wide ranges of ionic strengths and groundwater compositions, which subsequently was validated by an independent original dataset. This model improves the understanding of U(VI) retention by clay minerals and enables now predictive modeling of U(VI) sorption processes in complex clay rich natural environments.

Keywords: Argillaceous rock, Surface complexation modeling, Uranium, Specific ion interaction theory (SIT), ATR FT-IR, TRLFS

---

* Corresponding authors: Dr. Madlen Stockmann (E-mail address: m.stockmann@hzdr.de), Phone: +49 351 260 4675., Dr. Katja Schmeide (E-mail address: k.schmeide@hzdr.de), Phone: +49 351 260 2436.

E-mail addresses: katha.fritsch@googlemail.com (Katharina Fritsch), f.bok@hzdr.de (Frank Bok), maria.marques@psi.ch (Maria Marques Fernandes), bart.baeyens@psi.ch (Bartholomeus Baeyens), r.steudtner@hzdr.de (Robin Steudtner), k.mueller@hzdr.de (Katharina Müller), cordula@nebelungs.de (Cordula Nebelung), v.brendler@hzdr.de (Vinzenz Brendler), t.stumpf@hzdr.de (Thorsten Stumpf).

[1] Present address: Federal Office for the Safety of Nuclear Waste Management, 11513 Berlin.

1. Introduction

Radioactive waste generated in the nuclear energy production will preferably be stored in deep geological formations, where it has to be prevented from migrating towards the biosphere by technical, geotechnical and geological barriers. Argillaceous rocks are discussed in many countries as potential host rocks for deep geological repositories (ANDRA, 2005; Bock et al., 2010; Hoth et al., 2007; Nagra, 2002; Ojovan and Lee, 2005; ONDRAF/NIRAS, 2013), because of their favorable properties such as very low permeability, chemical buffering capability, high plasticity and swelling capacity ensuring self-sealing of potential fractures and fissures, and high retention capacities for contaminants and radionuclides. The clay mineral montmorillonite is a component of argillaceous host rocks and, moreover, the main component of bentonite, which is foreseen as a possible buffer and backfill material in high-level radioactive waste repository systems. In addition, as a ubiquitous mineral in nature, montmorillonite can contribute to the retention of (technologically enhanced) naturally occurring radioactive material (NORM), which includes uranium, resulting from activities such as burning coal, uranium mining, fertilizer production and use, as well as from oil and gas production (Al-Masri et al., 2019; IAEA, 2003; Papastefanou et al., 2000). Montmorillonite is a 2:1 phyllosilicate mineral composed of Al octahedral sheet sandwiched between two Si tetrahedral sheets (Grim, 1968; Van Olphen, 1966). It carries a permanent negative surface charge, arising from isomorphic substitutions in the octahedral, which is balanced by the presence of hydrated cations in the interlayer cation exchange. Adsorption at the clay-water interface occurs via cation exchange reaction in the interlayer and/or via surface complexation on the amphoteric hydroxyl edge sites (Sposito, 2008).

Spent fuel elements contain over 90 % uranium, with nearly 99% ^{238}U (half life $t_{1/2}$ = 4.468 × 10^9 a) and around 1% of remaining ^{235}U ($t_{1/2}$ = 7.038 × 10^8 a) and the activation product ^{236}U ($t_{1/2}$ = 2.342 × 10^7 a). Beside spent nuclear fuel and vitrified high-level waste, there are further potential sources of uranium contaminations such as uranium ore mining and processing, effluents from phosphate and rare earth production, the storage of long-lived intermediate-level and low-level waste, geothermal plants, and ammunition based on depleted uranium. Some of these uranium contamination sources relate to high ionic strength waters. In addition to its radiotoxicity, uranium also exhibits a high chemotoxicity. For any assessment of remediation measures, reduction of uranium release by technological processes or a safety case, knowledge about the retention of uranium by the surrounding soil and rock components is indispensable. Thermodynamic data that describe these processes are essential in reactive transport calculations, which are an integral part of such assessments.

Many studies have focused on the interaction of actinides with clay minerals at low ionic strengths, (Amayri et al., 2016; Bradbury and Baeyens, 2002; Catalano and Brown, 2005; Fralova et al., 2021; Glaus et al., 2020; Joseph et al., 2017; Joseph et al., 2013a; Joseph et al., 2013b; Křepelová et al., 2007; Meleshyn et al., 2009; Pabalan and Turner, 1997; Schmeide and Bernhard, 2010; Semenkova et al., 2018; Tran et al., 2018). In contrast to the clay rock-porewater systems investigated in Switzerland, France or Belgium (De Craen et al., 2004; Pearson et al., 2003; Vinsot et al., 2008), the electrolyte concentration in groundwaters of North German clay deposits is well above 1 mol L^{-1} (Brewitz, 1982). These groundwaters can reach ionic strengths up to 4 mol L^{-1} in the relevant depths, with calcium concentrations up to 0.6 mol L^{-1}. Furthermore, several measurements confirm the presence of significant amounts of HCO_3^-. Similar high ionic strengths are expected in potential sites for radioactive waste repositories in sedimentary rocks in Canada (Mazurek, 2004) and Japan (Hama et al., 2007).

Even within one specific site, electrolyte concentration and pH can vary depending on depth or mineral inventory. Both, ionic strength, which in turn has an influence on the activity coefficients of the ions in solution, and pH dependence of sorption processes, need to be investigated as they influence radionuclide speciation and sorption. Besides uranium, further fission and activation products are relevant, e.g., Am, Pu, and Np. Due to the high radiotoxicity of trivalent actinides and their difficulty handling in the lab, the lanthanides Ln(III) are often used as analogues with similar chemical behavior. Schnurr et al. (2015) investigated the Eu(III) and Cm(III) uptake onto illite and montmorillonite. They found no significant influence of ionic strength on Eu(III) uptake on illite above pH_c 6.5. On montmorillonite, the contribution of cation exchange to overall sorption is suppressed with increasing ionic strength and for pH_c values between 6 and 8-9, higher ionic strengths decrease Eu(III) sorption. Cm(III) was used as a fluorescence probe in laser fluorescence spectroscopy. It was found that the same Cm(III) surface species are present at low and high ionic strengths. The authors used literature values from (Bradbury and Baeyens, 2006, 2009) to model Eu(III) sorption and applied the Pitzer equations to account for the high ionic strength environment. For illite, the model considerably underpredicted sorption at higher ionic strengths, while for montmorillonite, the Eu(III) sorption curves could be reproduced more accurately. The authors ascribed this to the aggregation of montmorillonite at higher ionic strengths (cf. (Abend and Lagaly, 2000), which reduces the number of available surface sites. Marsac et al. (2017) investigated the uptake of Pu on illite du Puy. They found that Pu(IV) sorption onto illite is not influenced by ionic strength, while at $pH_c < 6$, where Pu(III) is the predominant oxidation state in solution, there is a decrease of Pu sorption with increasing ionic strength due to the ionic strength dependency of Pu^{3+}–Na^+ cation exchange. No evidence

was found for the precipitation of $PuO_{2\,(am,hydr)}$. Surface complexation modeling (SCM) was performed with the Specific Ion Interaction Theory (SIT) to account for the high ionic strengths. The authors used literature values for Pu(IV) sorption from Banik et al. (2016) and, as an analogue for Pu(III), Eu(III) surface complexation constants from Bradbury and Baeyens (2005). The experimental pH_c and pe of each data point were used as input due to the sensitivity of Pu redox speciation to these parameters. With the literature values and these parameters, Pu sorption was well reproduced. Poetsch and Lippold (2016) observed a strong decrease of Tb(III) and Eu(III) sorption on Opalinus Clay with increasing ionic strength. This effect was especially pronounced in $CaCl_2$ and $MgCl_2$ background electrolytes. Nagasaki et al. (2016) investigated Np(V) sorption on illite, shale and MX-80 montmorillonite in Na–Ca–Cl solutions in absence of CO_2. For the first two minerals they found that ionic strength had no significant influence on Np(V) uptake. On MX-80, Np(V) sorption decreased for ionic strength changes from 0.1 to 1 mol L^{-1}, with no significant ionic strength influence above 1 mol L^{-1}. Additionally, Np(V) sorption on all three sorbents was decreased by an increasing Ca^{2+} concentration in solution.

SCM, often in combination with ion exchange reactions, are used to quantitatively describe experimental adsorption results and to predict the retention of metal cations as well as anionic ligands onto solid phases (OECD/NEA, 2012; Payne et al., 2013). Such models use defined reactions between solution species and specific binding sites on mineral surfaces or even on biological matter (Ams et al., 2013). Several SCMs have been developed for simulating adsorption behavior of metals onto clay minerals, mostly differing in their treatment of the electric double layer (Bradbury and Baeyens, 1997; Grambow et al., 2006; Tertre et al., 2009; Tournassat et al., 2013; Tournassat et al., 2018), the number of surface protolysis steps, and the denticity and strengths of the binding sites. From these SCMs, the quasi-mechanistic two-site protolysis non-electrostatic surface complexation and cation exchange (2SPNE SC/CE) sorption model by Bradbury and Baeyens (1997) is the most often used model for argillaceous systems (see e.g. (Banik et al., 2016; Bradbury et al., 2005; Bruggeman et al., 2010; Cao et al., 2020; Ghayaza et al., 2011; Hartmann et al., 2008; Marsac et al., 2017; Schnurr et al., 2015; Sugiura et al., 2021)). It has been applied to U(VI) sorption by Bradbury and Baeyens (2005) and Marques Fernandes et al. (2012). In the former study, sorption of U(VI) and other trace metals on montmorillonite was modeled to determine a linear free energy relationship between aqueous hydrolysis constants and surface complexation constants. Surface complexation constants on strong and weak sorption sites and cation exchange coefficients for U(VI) sorption on several Na and Ca montmorillonites were derived, by which U(VI) sorption in the absence of CO_2 can be described in a wide pH range. The second study is

concerned with quantifying the influence of CO_2 on U(VI) sorption. For this, U(VI) sorption on Wyoming montmorillonite in the absence of CO_2, in the presence of micromolar amounts of HCO_3^- and under atmospheric conditions was modeled, using cation exchange and sorption on strong and weak edge sites. Two approaches were tested: (i) reducing aqueous uranyl carbonate complexation constants which yielded a bad fit (and was rejected) and (ii) considering the formation of uranyl carbonate surface complexes.

SCM requires a set of surface species. However, this assignment of surface species is usually based on a number of assumptions or even only on numerical "best fit" criteria. It does not necessarily reflect the true surface speciation in the experimental system nor follow the principle of parsimony, i.e. to choose the simplest model that can reasonably describe a given data set. Consequently, it is advisable to check these assumptions, e.g., disregarding surface precipitation of U(VI) as a U(VI) uptake mechanism, making the modeling more robust and reliable. In addition to a macroscopic description of surface reactions by means of distribution coefficients (K_d values), a detailed understanding of the prevalent species in solution and of the sorption mechanisms is crucial. Spectroscopic experiments are expected to provide such molecular structural information. Attenuated total reflection Fourier-transform infrared (ATR FT-IR) spectroscopy and time-resolved laser-induced fluorescence spectroscopy (TRLFS) offer an insight into the chemical environment of several lanthanides and actinides and enable an analysis of trace metal speciation in aqueous solution but also in situ at mineral-water interfaces (e.g. (Chang et al., 2006; Collins et al., 2011; Comarmond et al., 2016; Drobot et al., 2015; Marques Fernandes et al., 2016; Moulin et al., 1998; Müller et al., 2012; Neumann et al., 2021; Philipp et al., 2019; Rabung et al., 2005; Richter et al., 2016; Wolter et al., 2019b)). In particular, these spectroscopic methods are important tools to identify and characterize molecular species, e.g. giving hints to the number and formation of species being present simultaneously, stoichiometries in absence and presence of different ligands, to different types of surface complexes (inner-sphere, outer-sphere, oligomerization and precipitation) and thus, finally to validate thermodynamic and theoretical predictions.

A robust model to be applied for U(VI) interaction with clay in a broad variety of geochemical settings has to be able to describe these interactions over wide ranges of ionic strengths and groundwater compositions in general. Furthermore, such a model has to take competing cations (ref. e.g., (Marques Fernandes and Baeyens, 2020)) into account, e.g. alkaline earth ions, as they not only contribute to the overall ionic strength but might affect the aqueous speciation, can sorb themselves on the mineral, thus blocking binding sites, and might induce (co-)precipitation. The impact of calcium (Ca^{2+}) is one of the important issues in long-term safety assessment of repositories and has been studied e.g. by Hennig et al. (2020), Missana and Garcia-Gutierrez (2007), Philipp

et al. (2019), Richter et al. (2016), Sugiura et al. (2021), Szymanek et al. (2021), and Wolter et al. (2019a). And last but not least, the set of thermodynamic parameters used needs to be internally consistent. This is most easily achieved by simultaneously fitting all raw experimental data to the full model, as is done in this work.

The aim of this study was a systematic investigation and description of the influence of ionic strength and various types of background electrolytes (NaCl and $CaCl_2$) on the retention processes of U(VI) by the clay mineral montmorillonite. Therefore, U(VI) speciation in high ionic strength solutions and U(VI) sorption onto montmorillonite at increased salinities were investigated by batch sorption experiments and spectroscopic methods (TRLFS, ATR FT-IR). The experimental data of this study and published batch sorption data from comparable experimental U(VI) sorption studies on montmorillonite were used to develop a comprehensive SCM, that describes pH dependent sorption (edges) in various background electrolytes, to improve our understanding of U(VI) retention by clay minerals. Finally, to verify the robustness of the derived model, a blind prediction of additional uranium sorption data that was not part of the fit pool was performed and compared to the reported sorption curves.

2. Materials and methods

2.1. Materials

A Na-montmorillonite (SWy-2, Crook County, WY, USA) was used as model clay mineral. It was purified according to Baeyens and Bradbury (1997). This purification consists of transforming the clay into its Na-form and elimination of soluble salts and solid phases (*e.g.* carbonates), a size separation step to enrich the < 0.5 µm fraction, an acidification step to eliminate hydroxides of low solubility and lastly a dialysis against deionized water (until a residual conductivity of ≤ 10 S cm^{-1} was achieved) and a freeze-drying step. The purified clay was then analyzed by inductively coupled plasma mass spectrometry (ICP-MS, mod. ELAN 9000, Perkin Elmer, Waltham, MA, USA) after microwave digestion to obtain the phase composition (cf. Table S1 in the Supplementary Information - SI). X-ray diffraction (XRD, mod. Diffractometer D8, Bruker AXS GmbH, Karlsruhe, Germany) yielded diffractograms that closely resemble the reference patterns for size-separated SWy montmorillonite (not shown, Chipera and Bish (2001)). Furthermore, the specific surface area (SSA) was determined by the N_2-Brunauer-Emmett-Teller (BET) method (mod. Coulter SA 3100, Beckman Coulter, Brea, CA, USA) and yielded a SSA of 41.1 ± 0.8 m^2 g^{-1}.

A $^{238}U(VI)$ stock solution (5×10^{-4} mol L^{-1} $^{238}UO_2Cl_2$ in 0.01 mol L^{-1} HCl) was used for all experiments. To prepare the background electrolyte, NaCl (p.a., ≥ 99.5 %, Roth, Karlsruhe, Germany) or $CaCl_2 \cdot 2H_2O$

(p.a., Merck, Darmstadt, Germany) was dissolved in deionized water (18 MΩ cm^{-1}; mod. Milli-RO/Milli-Q-System, Millipore, Schwalbach, Germany).

The pH values were adjusted with diluted HCl (Roth) and NaOH (p.a., Merck) (0.01 or 0.1 mol L^{-1} each). For experiments in absence of CO_2, NaOH prepared from rinsed NaOH pellets (p.a., Roth) was used. The pH values were measured with laboratory pH meters (inoLab pH 720, WTW, Weilheim, Germany and pMX 3000/pH coupled with Multiplex 3000/pMX, WTW) with SenTix®Mic pH microelectrodes (WTW), calibrated with standard buffers at pH 1.679, 4.006, 6.865 (WTW) and 9.18 (Hanna Instruments, Woonsocket, RI, USA).

At high ionic strength, the usage of pH as the negative decadic logarithm of the hydrogen ion activity is not feasible due to the strong dependency of activity on ionic strength. Instead, pH_c is used, the negative decadic logarithm of the molal hydrogen concentration. For practical measurement, a correction function that correlates the value displayed by the pH meter (pH_{exp}) with the pH_c is applied. For this, the approximations recommended by Altmaier et al. (2003) and Altmaier et al. (2008) were used.

2.2. Batch sorption experiments

For the batch sorption experiments, 40 mg of the purified montmorillonite were weighed into 15 ml centrifuge tubes (PP, Cellstar, Greiner Bio-One GmbH, Frickenhausen, Germany). Then, pre-calculated amounts of NaCl or $CaCl_2$ were weighed to the clay. The batch sorption experiments were carried out as function of pH_c (NaCl: 4 - 10; $CaCl_2$: 4 - 9) and ionic strength (0.1 - 3 mol kg^{-1}). The experimental conditions are summarized in Table S2 in SI.

For the experiments under well-controlled ambient conditions ($p_{CO_2} = 10^{-3.5}$ atm, T = (23 ± 2) °C), 8.5 g of deionized water were added. Then, pre-calculated amounts of 1 mol L^{-1} $NaHCO_3$ (> 99.5 %, p.a, Merck) were added to achieve near-instant equilibrium with atmospheric CO_2. The samples were shaken continuously in an overhead shaker (mod. Reax 20, Heidolph, Schwabach, Germany). The samples were pre-equilibrated for 10 days (NaCl) or 4.5 weeks ($CaCl_2$), during which pH_c was adjusted frequently until pH_c stability was reached. Then, further deionized water was added so that the samples contained 10 g of water each (solid-liquid ratio, SLR: 4 g kg_{water}^{-1}). After an additional pH_c adjustment, an aliquot of U(VI) stock solution was added to achieve the initial U(VI) concentration ($c_{m,U(VI)} = 1 \times 10^{-6}$ mol kg^{-1}). After 4 to 7 days, during which pH_c was repeatedly adjusted, the sorption step was completed, as shown by preliminary experiments (cf. Section 3.2).

Samples equilibrated under CO_2-free conditions were transferred into a N_2-glove box (T = (23 ± 2) °C), where 8.5 g of degassed deionized water were added. The samples were loaded into an air-proof shaking vessel

and transferred to an overhead shaker. Pre-equilibration took 4.5 weeks with frequent pH_c adjustments until pH_c stability (± 0.2) was reached, after which the samples were filled up to contain 10 g of water in total. Following an additional pH_c adjustment, U(VI) stock solution was added to achieve the initial U(VI) concentration ($c_{m,U(VI)} = 1 \times 10^{-6}$ mol kg^{-1}). Sorption was found complete after 1 week, with frequent pH_c adjustments during this week, which affected the overall SLR to less than 2 %. This was backed by sorption kinetic experiments (cf. Fig. S1 in SI) with 18 single data points performed at pH_c 5.3 with an initial ^{238}U(VI) concentration of 1×10^{-6} mol kg^{-1}, a SLR of 4 g kg^{-1}_{water} and an ionic strength of 2 mol kg^{-1} NaCl under ambient CO_2 conditions. Sorption times ranged from 30 minutes to 1 week, with 10 data points on the first day of sorption.

When sorption was complete, the samples were centrifuged (mod. Avanti J-20XP, Beckman Coulter, Brea, CA, USA, 30 min, 4500×*g*) and then filtered (PES syringe filter, 0.2 µm, vwr, Radnor, PA, USA) into new centrifuge tubes. Photon correlation spectroscopy (mod. BI90, Brookhaven Instruments, Holtsville, NY, USA) showed that this treatment was sufficient to remove colloids. Subsequently, an aliquot of the solution was acidified to 1 % HNO_3 and analyzed for U by ICP-MS. Analysis for Na and Ca was done by flame atomic absorption spectroscopy (F-AAS, mod. AAS-4100, Perkin Elmer). Ion chromatography (mod. IC Separation Center 733, IC Detector 732, Deutsche Metrohm GmbH & Co. KG, Filderstadt, Germany) was used to determine chloride and carbonate content in solution. Container wall sorption was determined by shaking the empty vials used in the batch sorption experiments afterwards with 1 mol L^{-1} HNO_3, with subsequent analysis for U by ICP-MS.

Parallel to the ionic strength and pH_c dependency experiments, leaching experiments without addition of U(VI) and control experiments without clay mineral were performed (single data points, not shown here). The conditions were identical to the sorption experiments. After completion, the solutions were analyzed for Na, Mg, Al, Si, P, K, Ca, Ti, Mn, Fe, and U by ICP-MS and AAS.

2.3. Spectroscopic methods

To check the theoretically calculated aqueous U(VI) speciation and to study U(VI) sorption on molecular level, TRLFS and *in situ* ATR FT-IR spectroscopy, respectively, were applied.

2.3.1. Time-resolved laser-induced fluorescence spectroscopy (TRLFS)

In a first attempt, TRLFS was tested to identify U(VI) surface species on montmorillonite. However, the very noisy spectra obtained, also due to severe quenching by the solid and the missing signals from carbonate species did not allow any sensible speciation analysis. But it was decided to utilize TRLFS at least to identify U(VI) species in 3 mol kg^{-1} NaCl and 1 mol kg^{-1} $CaCl_2$ solutions in absence and presence of CO_2 as a function of pH_c. Apart from UO_2CO_3, the uranyl carbonate complexes do not show fluorescence at room temperature (Wang et al., 2004). Due to this and because of an increase of fluorescence intensity providing access to lower U(VI) concentrations, the TRLFS measurements were conducted at cryogenic conditions. The spectral resolution will also increase (Wang et al., 2008). The U(VI) solution (1×10^{-6} mol kg^{-1}) was filled into plastic cuvettes (polystyrene one-time cuvette, Roth) and shock frozen with liquid nitrogen. These samples were attached to a sample holder and cooled down to 153 K by using a cryogenic cooling system (mod. TG-KKK, KGW-Isotherm, Karlsruhe, Germany). The U(VI) luminescence was measured using a Nd:YAG laser system (mod. Minilite, Continuum, Santa Clara, CA, USA) as described in Steudtner et al. (2011), after excitation with laser pulses at 266 nm with an averaged pulse energy of 1 mJ. The emitted luminescence light of the samples was recorded with a spectrograph (mod. iHR 550, HORIBA Jobin Yvon, Unterhaching, Germany) and an ICCD camera (mod. ICCD-3000, HORIBA Jobin Yvon) in the wavelength range from 369.8 to 669.2 nm by accumulating 250 laser pulses and using a gate time of 200 µs. Time-resolved spectra were recorded by measuring at dynamic delay times t_i (µs), which were calculated according to the following equation.

$$t_i = i + \frac{i^4}{300} \quad (1)$$

where i stands for the number of steps in series. An average of 50 measurements was used for each delay time.

2.3.2. In situ attenuated total reflection Fourier-transform infrared (ATR FT-IR) spectroscopy

Infrared spectra were measured on a Vertex 80/v vacuum spectrometer (Bruker) equipped with a Mercury Cadmium Telluride (MCT) detector. Spectral resolution was 4 cm^{-1} and spectra were averaged over 256 scans. The ATR accessory DURA SamplIR II (Smiths Detection, Watford, Herts, UK) used here is a horizontal diamond crystal (A = 12.57 mm^2) with nine internal reflections on the upper surface and an angle of incidence of 45°. The IR measurements were based on the principle of reaction-induced difference spectroscopy that has been previously described in Müller et al. (2012) and Müller et al. (2013). In short, after pre-equilibration of montmorillonite in a diluted NaCl solution for 1 week, the 2.5 g L^{-1} montmorillonite suspension was deposited on the ATR crystal as stationary phase until a film density of approximately 0.05 mg cm^{-2} was achieved. The

film was then flushed with solutions containing the background electrolyte at a certain pH with and without U(VI). Changes at surface were monitored with a sub-minute time resolution by recording single-beam spectra. Difference spectra were calculated at distinct time intervals.

The IR measurements were performed in 3 and 0.3 mol L^{-1} NaCl, at pH_c 6.8, under N_2 atmosphere. However, IR measurements in presence of CO_2 were not evaluable as explained in Section 3.3. To increase the signal-to-noise ratio, D_2O was used instead of H_2O. The U(VI) concentration in the sorption step (2×10^{-5} mol L^{-1}) was slightly higher than that used in the batch sorption experiments. This ensures that a decent signal-to-noise ratio for the evaluation of the surface complexes is achieved while the U(VI) speciation in solution is still reasonably similar to solutions with 1×10^{-6} mol L^{-1} U(VI) (cf. Section 3.3). Signals from precipitates were not detectable in the IR spectrum and can be excluded. They are distinguished from surface complexes and aquatic species by their appearance at particular frequency (~ 940 cm^{-1}) as sharp and intense peaks.

2.4. Surface complexation modeling and parameter derivation

The derivation of the surface complexation parameters was performed with the geochemical speciation code PHREEQC version 3.5.2 (Parkhurst and Appelo, 2013) coupled with the parameter estimation program UCODE 2014 version 1.004 (Poeter et al., 2014). Thermodynamic parameters were taken from the PSI/Nagra thermodynamic database version 12/07 (Thoenen et al., 2014). This database included uranium data based on the NEA TDB (Guillaumont et al., 2003) and was updated as necessary e.g. for calcium uranyl carbonates from the THEREDA Release 2020 (www.thereda.de) or the NEA Second Update, Vol. 14 (Grenthe et al., 2020) as given in Tables S3 and S4 in SI. The aqueous chemical speciation of U(VI) was calculated in equilibrium with montmorillonite as well as with the carbonate concentration as given by the original publications (p_{CO_2} = $10^{-3.5}$ atm). The solubility product for a Na-montmorillonite (type: Montmorillonite-BCNa with the formula $Na_{0.34}Mg_{0.34}Al_{1.66}Si_4O_{10}(OH)_2$) was taken from the latest version of the ANDRA Thermodynamic Database (ThermoChimie-TDB_v10a, (Giffaut et al., 2014)). The formation of crystalline U(VI) phases was not considered due to the relatively short duration of the sorption experiments (< 7 days). However, due to the high ionic strengths (up to 3 mol kg^{-1}), more amorphous solid phases such as metaschoepite ($UO_3{:}2H_2O$), Na-compreignacite ($Na_2(UO_2)_6O_4(OH)_6{:}7H_2O$) or clarkeite ($Na(UO_2)O(OH)$) could precipitate and were consequently checked in our model. Thereby, the solubility product for clarkeite was taken from Gorman-Lewis et al. (2008) with log $K°$ = 9.4. This value is derived from solubility experiments with lower reaction

time and points rather to amorphous phases. For the $CaCl_2$ system, the precipitation of calcite was expected and considered in the model. Here too, it is unlikely that in the relatively short time of seven days in which U(VI) was present in solution, potential Ca-U(VI) solid phases such as becquerelite (CaU_6O_{19}:$11H_2O$) were formed.

To correct the activity coefficient γ for higher ionic strengths (up to 3 mol kg^{-1} in this work) the Specific Ion Interaction Theory (SIT) (Guggenheim and Turgeon, 1955) was used in modeling calculations. However, no interaction coefficients between negatively charged uranyl hydroxides or uranyl carbonates and Ca^{2+} are available in the literature, decreasing the accuracy of the calculated U(VI) speciation under these high ionic strength conditions. All relevant thermodynamic data for the formation of aqueous species and solid phases for U(VI) as well as SIT ion interaction coefficients ε (kg mol^{-1}) used in this work were mainly taken from the PSI/Nagra thermodynamic database version 12/07 (Thoenen et al., 2014) and are compiled in Tables S3 and S4 in SI.

To consider the sorption of U(VI) onto montmorillonite (surface complexation and cation exchange reactions), the 2SPNE SC/CE model (Bradbury and Baeyens, 1997) was used. This model combines SCM and ion exchange. It disregards electrostatic effects and uses two types of surface binding sites: One, strong ($\equiv S^SOH$), with a high affinity site but a lower overall site capacity, and another more numerous site types, weak ($\equiv S^{W1/W2}OH$), with lower sorption affinity. In case of trace metal sorption, cations will mainly bind to the strong sites and only when the strong sites begin to saturate at higher metal concentrations, cation uptake will also take place on the weak sites. Based on this 2SPNE SC/CE model we developed a specific SCM model for U(VI) sorption on montmorillonite (U(VI) model) tailored to the precise conditions encountered in the present experiments. The U(VI) concentrations lie below the sorption site capacity for strong sorption sites: at a SLR of 4 g_{clay} kg_{water}^{-1} and a surface site capacity of 2×10^{-3} mol kg_{clay}^{-1} (cf. Table 1), the number of available strong surface sorption sites is 8×10^{-6} mol kg_{water}^{-1}, which is 8 times larger than the initial U(VI) concentration in solution, 1×10^{-6} mol kg^{-1}. Therefore, we focused on the strong sites for SCM parameter derivation. Surface complexes on weak sorption sites can be discounted completely under these conditions, as was also done by Bradbury and Baeyens (2009). The surface site capacities and protolysis constants for montmorillonite derived by Bradbury and Baeyens (1997) were used as non-adjustable parameters in the surface complexation model in this work (cf. Table 1). The SSA, as determined in the present study is given in Table S2 in SI. The cation exchange capacity (CEC), the cation exchange reactions and corresponding selective coefficients (K_c Na/U and Na/Ca) are considered as further non-adjustable parameters as given in Table 1.

Table 1: Summary of site types, surface site capacities and protolysis constants for Na-montmorillonite (Bradbury and Baeyens, 1997) as well as cation exchange reactions for Na/U (Bradbury and Baeyens, 2005) and Na/Ca (Bradbury and Baeyens, 1999) used as non-adjustable parameters in this work.

Site types	Site capacity
$\equiv S^{S}OH$	2×10^{-3} mol kg^{-1}
$\equiv S^{W1/W2}OH$	4×10^{-2} mol kg^{-1}
Cation exchange capacity	8.7×10^{-1} eq kg^{-1}
Surface protolysis reactions	log $K°$
$\equiv S^{S,W1}OH + H^+ \rightleftharpoons \equiv S^{S,W1}OH_2^+$	4.5
$\equiv S^{S,W1}OH \rightleftharpoons \equiv S^{S,W1}O^- + H^+$	-7.9
$\equiv S^{W2}OH + H^+ \rightleftharpoons \equiv S^{W2}OH_2^+$	6.0
$\equiv S^{W2}OH \rightleftharpoons \equiv S^{W2}O^- + H^+$	-10.5
Cation exchange reaction	log K_c
$2Na\text{-clay} + Ca^{2+} \rightleftharpoons Ca^{2+}\text{-clay} + 2Na^+$	0.61
$2Na\text{-clay} + UO_2^{2+} \rightleftharpoons UO_2^{2+}\text{-clay} + 2Na^+$	0.15

To develop a robust U(VI)-model able to describe properly a wide range of geochemical conditions, the following experimental data from different studies on U(VI) sorption onto montmorillonite were aggregated: a) the experimental data of the present work (NaCl and $CaCl_2$ system), and b) U(VI) sorption data obtained from Nebelung et al. (2007), Marques Fernandes et al. (2012) as well as Bradbury and Baeyens (2005). However, in the presence of CO_2 the system buffers since the NaOH is then completely converted to Na_2CO_3 solution by the CO_2 intrusion due to the carbonation reaction ($2Na^+ + 2OH^- + CO_2(g) = 2Na^+ + CO_3^{2-} + H_2O$). Therefore, all data points with pH > 9.5 were excluded in the carbonate-containing NaCl systems. Furthermore, two data points at pH_c 8 at I = 0.3 mol kg^{-1} in the CO_2-free $CaCl_2$ sample series (marked with grey dots in Fig. 3) were excluded from the fit due to suspected carbonate content in these samples. For the experimental data of Nebelung et al. (2007) a deviation from the data of the carbonate-containing systems of this work and Marques Fernandes et al. (2012) can be seen in the alkaline range above pH > 6. This could be due to several reasons, such as an increased carbonate content or an increased Ca content in the system due to impurities in the samples, which leads to an increased formation of the aquatic calcium uranyl carbonate species and a decreased U(VI) sorption. Therefore, 8 data points above pH_c > 6 from Nebelung et al. (2007) were excluded

from the fit (marked with grey dots in Fig. 5). This provided 213 experimental data points in total to derive the surface complexation constants (log $K°$ values).

The experimental sorption values were defined as sum of sorbed and potentially precipitated percentage (U(VI) immobilized in %). The quantification of sorption in this form was preferred against K_d values or total concentrations as it provides implicitly a data weighing that mimics analytical uncertainties – remember that the primary ICP-MS result always is concentration of U(VI) remaining in the aqueous phase. All experimental boundary conditions, such as ionic strength, background electrolyte, pH range, initial U(VI) concentration, SLR, SSA, and absence or presence of CO_2, were considered in the SCM model, for their values cf. Table S2 in SI. As we assumed that the systems were in equilibrium, kinetic processes were not considered. The leaching experiments (not depicted) showed that the leachable U(VI) content in the montmorillonite did not affect the parameter estimation process and was therefore eliminated in an effort to keep the model as simple as possible. Container wall sorption was not included in the calculations, as it was also found to be negligible.

The fitting procedure utilized a combination of the codes PHREEQC and UCODE. A weighted residuals model was used to find the best fit. Thereby, the quality of the fit is assessed on the basis of the calculated error variance (CEV) as well as the standard deviation of the final log $K°$ values as output parameter of UCODE (Poeter et al., 2014). The CEV is calculated by the sum of squared weighted residuals divided by the number of observations (here 213 experimental data points) minus the number of estimated parameters (here 3-4 surface complexation constants).

3. Results and discussion

3.1. Aqueous U(VI) speciation

The calculated aqueous U(VI) speciation in the NaCl and $CaCl_2$ electrolytes in the absence and presence of CO_2 is shown in Figs. S2 and S3 in SI for I = 3 mol kg^{-1}. The free uranyl cation, UO_2^{2+}, and uranyl chlorides are the dominant species up to pH_c 5.5. In absence of CO_2 in both electrolytes, U(VI) forms various uranyl hydroxide species above pH_c 5.5, whereas in presence of CO_2 in NaCl uranyl carbonates dominate the speciation in the circumneutral and alkaline pH_c range. In $CaCl_2$, U(VI) predominantly forms the $Ca_2UO_2(CO_3)_{3(aq)}$ complex. An ionic strength effect can be observed for the formation of the $Ca_2UO_2(CO_3)_{3(aq)}$ complex in solution. Measurements of the carbonate content in samples with $CaCl_2$ as electrolyte showed a decrease in carbonate content with increasing pH_c. In the speciation and surface complexation calculations, the carbonate content in solution was therefore calculated by equilibrating the solution with air, followed by a

calcite precipitation step before the sorption step. The kinetic of calcite precipitation is well-described and reviewed by Morse et al. (2007) and takes effect at $pH_c > 7$. Backdiffusion of CO_2 was obviously slow in the experiments, so the carbonate content in solution turned small enough that uranyl hydroxides became once again the dominant U(VI) species at pH_c 8.5.

In a second step, the calculated aqueous U(VI) speciation was spectroscopically checked and broadly confirmed at selected pH_c values both in absence and presence of CO_2 by TRLFS. The fluorescence emission spectra of the U(VI) solutions measured at 153 K are shown in Fig. 1 (NaCl) and Fig. 2 ($CaCl_2$) with the band positions reported in Tables S5 to S7 in SI.

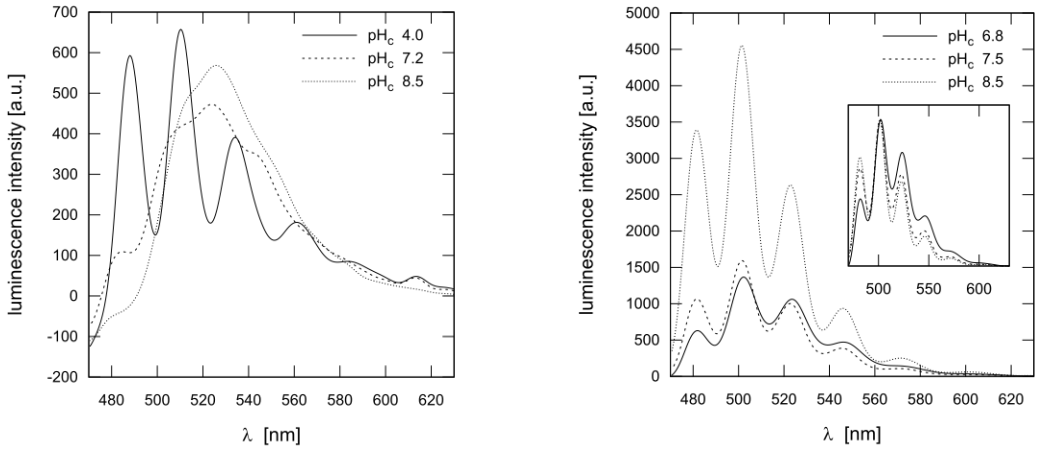

Fig. 1: Cryo-TRLFS spectra of U(VI) ($c_{m,U(VI)} = 1 \times 10^{-6}$ mol kg^{-1}) in 3 mol kg^{-1} NaCl in absence (left) and presence (right) of CO_2 as a function of pH_c. Inset: Spectra normalized to maximum luminescence intensity.

As shown in Fig. 1 (left), the spectrum in 3 mol kg^{-1} NaCl in the absence of CO_2 at pH_c 4 reflects exactly the band position of the free UO_2^{2+} ion (cf. Table S5 in SI). With increasing pH_c, a shift of the band positions towards higher wavelengths as well as a loss in fine structure can be observed. These changes in the luminescence spectra are typical for the formation of U(VI) hydrolysis species ((Drobot et al., 2015; Steudtner et al., 2010) and references therein). However, an assignment of distinct species by peak positions as well as fluorescence lifetime is not possible due to a lack of reference literature spectra of uranyl hydroxides recorded at cryogenic conditions comparable to those of this study. The spectra recorded in presence of CO_2 (cf. Fig. 1, right) are clearly distinguished from the CO_2-free system. These spectra are shifted to lower wavelengths in comparison to the free UO_2^{2+} ion (cf. Table S6 in SI), whereas the fine structure remains unaffected. At pH_c 8.5 the emission band positions correspond to literature values for $UO_2(CO_3)_3^{4-}$ (Götz et al., 2011; Wang et al., 2004). With decreasing pH_c value, the luminescence signal decreases, the peak ratios are changing and the

fluorescence lifetimes shorten. At pH_c 6.8, the TRLFS spectrum corresponds to published spectra assigned to UO_2CO_3 (Wang et al., 2004), with a strong red-shift of 30 nm compared to the free uranyl ion. However, according to the U(VI) speciation calculations, the $(UO_2)_2CO_3(OH)_3^-$ complex should be the dominant U(VI) species at this pH_c (cf. Fig. S2 in SI). This discrepancy between thermodynamics and spectra assignment cannot be resolved at the moment and calls for a more systematic spectroscopic investigation of binary and ternary U(VI) carbonate complexes.

In 1 mol kg^{-1} $CaCl_2$, spectra were recorded in presence of CO_2 (cf. Fig. 2). The fluorescence lifetimes of around 1 ms and the emission band positions (cf. Table S7 in SI), which are shifted to even lower wavelengths than the spectra for uranyl carbonates found in absence of calcium, correspond to the spectral data of $Ca_2UO_2(CO_3)_{3(aq)}$ (Wang et al., 2004). This effect of Ca^{2+} on U(VI) speciation, connected with a decrease of U(VI) sorption, can be observed already at millimolar concentrations of Ca^{2+} and will certainly be observed in high ionic strength groundwaters with Ca^{2+} concentrations in the order of hundreds of millimolar and presence of HCO_3^- in solution (Philipp et al., 2019; Richter et al., 2016; Shang and Reiller, 2020). The reduced fluorescence intensity of the TRLFS spectrum at pH_c 9.0 compared to pH_c 7.5 at identical U(VI) concentrations confirms the reduced fraction of $Ca_2UO_2(CO_3)_{3(aq)}$ in the U(VI) solution speciation in the higher pH_c range. However, any suspected uranyl hydroxides could not be identified in this spectrum due to the much larger relative fluorescence intensity of $Ca_2UO_2(CO_3)_{3(aq)}$.

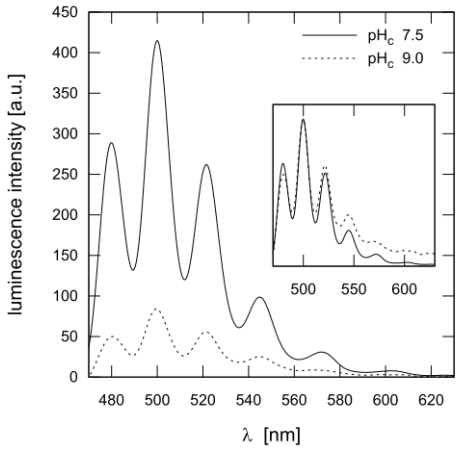

Fig. 2: Cryo-TRLFS spectra of U(VI) ($c_{m,U(VI)}$ = 1 × 10^{-6} mol kg^{-1}) in 1 mol kg^{-1} $CaCl_2$ in presence of CO_2 as a function of pH_c. Inset: Spectra normalized to maximum luminescence intensity.

3.2. U(VI) sorption onto montmorillonite as function of pH_c, CO_2 and ionic strength

The results of the kinetic experiments showed that sorption was constant already after 4 hours (cf. Fig. S1 in SI) and remained so for at least 168 hours. In fact, the sorption process is fast enough that a relative sorption of 90 % was reached in less than 30 min. Nevertheless, for the pH_c and ionic strength dependency experiments, longer sorption times were chosen to allow the detection of possible effects that may manifest within days instead of hours. In Fig. 3, the results of the pH_c dependent U(VI) sorption onto montmorillonite are presented for the NaCl and $CaCl_2$ systems for the different ionic strengths. The curves overlaying the experimental data points are surface complexation curves calculated from the derived surface complexation constants as described in Section 3.4. The individual surface complexes SC-1 to SC-3 are shown exemplarily for I = 0.3 mol kg^{-1} in Fig. S4 in SI.

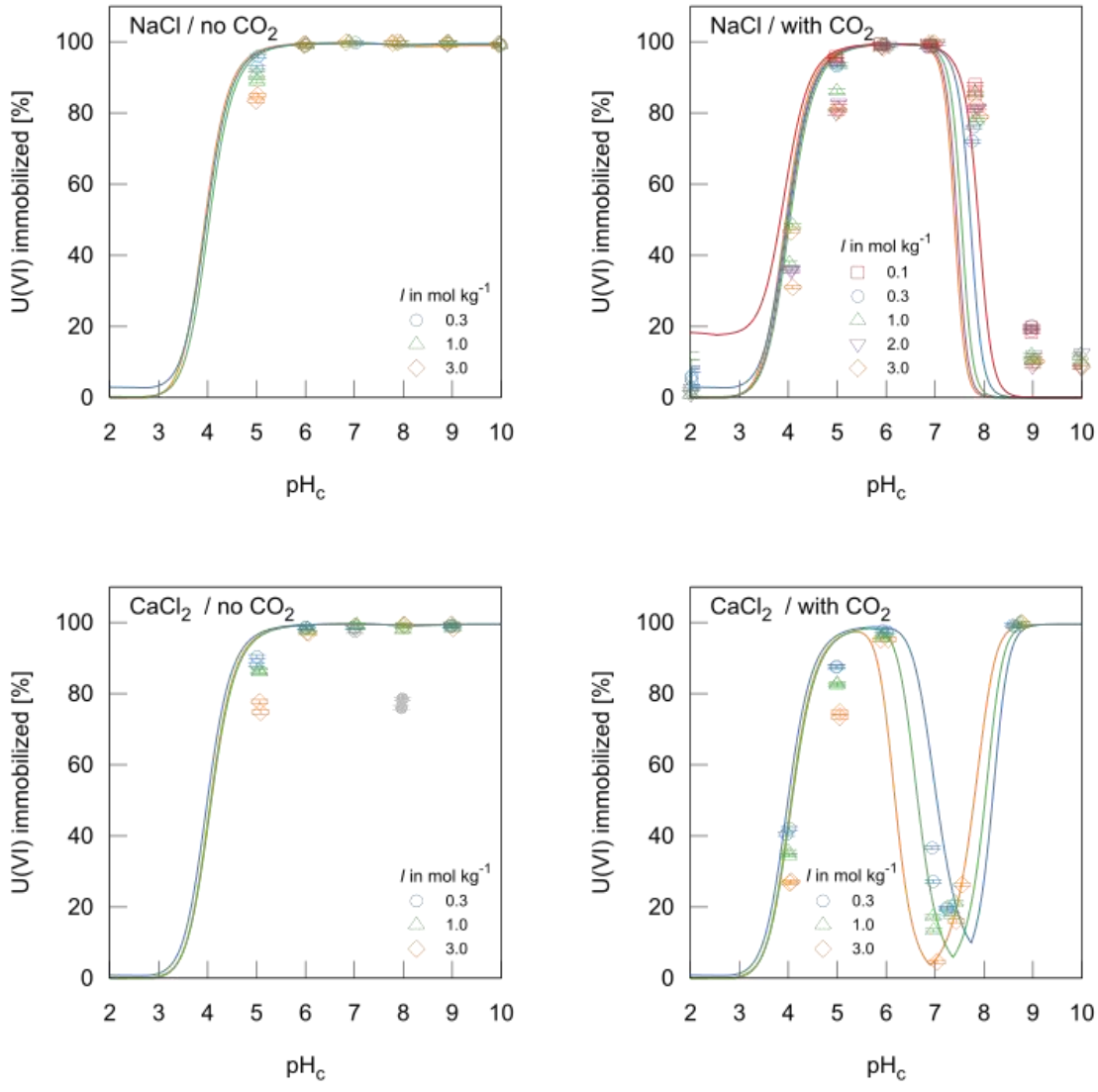

Fig. 3: U(VI) experimental batch sorption data for montmorillonite (symbols) and simulated results using the SCM model without ternary U-CO_3-surface complex (SCM-A) (lines) for NaCl (above) and $CaCl_2$ (below) ($c_{m,U(VI)}$ = 1 × 10^{-6} mol kg^{-1}) as a function of pH_c and ionic strength in absence (left) and presence (right) of CO_2 (p_{CO_2} = $10^{-3.5}$ atm). (Marked with grey dots: Outlier as explained in Section 2.4).

The shape of the sorption edges for the NaCl system is in good agreement with results of comparable studies of U(VI) adsorption on montmorillonite (Bradbury and Baeyens, 2005; Marques Fernandes et al., 2012; Nebelung et al., 2007) as illustrated in Fig. 5. Below pH_c 4 at low ionic strength, U(VI) is sorbing primarily to cation exchange sites in the interlayer. At high ionic strengths, cation exchange is strongly reduced, and from pH_c 4 onwards sorption is taking place mainly at the edge sites of montmorillonite. For pH_c > 4 an increasing U(VI) retention is observed caused by pH_c-dependent surface complexation reactions due to the enhanced deprotonation of the surface sites. For the CO_2-free NaCl system, a complete U(VI) sorption occurs above pH_c 6. In the presence of carbonate, the sorption maximum is between pH_c 6 and 7.5 and a very slight increase in U(VI) sorption with ionic strength was observed both in the absence and presence of CO_2 as verified in the ATR FT-IR *in situ* sorption experiment (cf. Section 3.3). In the alkaline pH_c range aqueous U(VI) carbonate complexes dominate and lead to a decrease of U(VI) retention above pH_c 7.5. A slight deviation can be seen at pH > 9 which could be due to a reduced carbonate content in the experiments. The precipitation of Na-U(VI)-solid phases such as metaschoepite (UO_3:$2H_2O$), Na-compreignacite ($Na_2(UO_2)_6O_4(OH)_6$:$7H_2O$) or clarkeite ($Na(UO_2)O(OH)$) is not considered because a complete formation of such solid phases is not expected within the relatively short time of our seven-days sorption experiments.

The shape of the sorption edges for the $CaCl_2$ system is comparable to the NaCl system. Above pH_c 4 an increasing U(VI) retention is observed, with maximum values above pH_c 6 in the absence of carbonate. The sorption values above pH_c 6 are slightly lower than in the respective NaCl system, which is due to a slight competition of Ca^{2+} and UO_2^{2+} for sorption sites. In the presence of carbonate, U(VI) sorption decreases sharply between pH_c 6 and 7. This is due to the formation of the strong aqueous $Ca_2UO_2(CO_3)_3$ complex which reduces U(VI) sorption to a much higher extent than the $UO_2(CO_3)_x^{(2-2x)}$ complexes occurring in the NaCl system (Fig. 3, right). This is confirmed by our TRLFS measurements and is in accordance with thermodynamic modeling (Fig. 2 and Figs. S2 and S3 in SI). The strong sorption decreasing effect of $Ca_2UO_2(CO_3)_{3(aq)}$ agrees with literature data (Dong et al., 2005; Joseph et al., 2013a; Meleshyn et al., 2009; Philipp et al., 2019; Schmeide et al., 2014; Zheng et al., 2003). The mobility of this uncharged species in clay rock was verified by diffusion and modeling studies (Joseph et al., 2013b; Xiong et al., 2015). The ionic strength dependence observed for the sharp decrease in sorption at pH_c > 6 is attributed to the shift of the $Ca_2UO_2(CO_3)_{3(aq)}$

dominance region to lower pH values with increasing Ca^{2+} concentration in solution associated with concomitant increasing ionic strength, as reported by Shang and Reiller (2020). This is supported by our U(VI) speciation calculations performed for I = 0.3 and 3 mol kg^{-1} ($CaCl_2$) (cf. Fig. S3 in SI). Under alkaline conditions, the U(VI) retention increases again due to precipitation of calcite ($CaCO_3$), which reduces the carbonate content in solution. This leads to a decreasing fraction of uranyl carbonate species and an increasing fraction of uranyl hydroxide species, as discussed in Section 3.1. The precipitation of Ca-U(VI)-solid phases such as becquerelite (CaU_6O_{19}:$11H_2O$) is not considered because the TRLFS measurement of 1×10^{-6} mol kg^{-1} U(VI) in 1 mol kg^{-1} $CaCl_2$ at pH_c 9 (cf. Section 3.1) did not show evidence for the formation of a U(VI) precipitate suspended in solution. It is unlikely that in the relatively short time of seven days in which U(VI) was present in solution, an equilibrium with the potentially formed U(VI) precipitate was reached.

3.3. In situ ATR FT-IR spectroscopic characterization of the sorption reaction

Fig. 4 (left) illustrates the course of a time-resolved ATR FT-IR *in situ* sorption experiment. The difference spectrum obtained from 60 min conditioning with blank solution reflects a sufficient stability of the montmorillonite film prepared as stationary phase on the ATR crystal (Fig. 4, left, lower trace). Nevertheless, there was some out-flushing of clay particles, which manifests in the bands visible in the > 1000 cm^{-1} wavenumber range. The time-resolved spectra of the sorption stage (Fig. 4, left, middle traces) are characterized by an increasing band amplitude reflecting U(VI) accumulation on the mineral surface with ongoing sorption time. In the IR spectra, the antisymmetric stretching vibrational mode ν_3 of the U(VI) moiety can be observed. The free uranyl cation in solution shows an absorption band of the $\nu_3(UO_2^{2+})$ mode at 961 cm^{-1} (Quilès and Burneau, 2000). Upon complexation in solution, e.g. with inorganic ions, or at mineral water interfaces the ν_3 mode shifts to lower wavenumbers because of a decrease of the U=O force constant. At a U(VI) concentration of 0.1 mol L^{-1} (pH ≈ 4), Quilès and Burneau (2000) found $(UO_2)_3(OH)_5^+$ to be the dominant uranyl species in solution, characterized by an absorption band at 923 cm^{-1}. At a considerably reduced U(VI) concentration of 2×10^{-5} mol L^{-1} at the same pH value of 4, the formation of a monomeric species was proposed with a very similar spectral response of ν_3 at 922 cm^{-1}, which was assigned to stem from the $UO_2(OH)_2$ species (Müller et al., 2008).

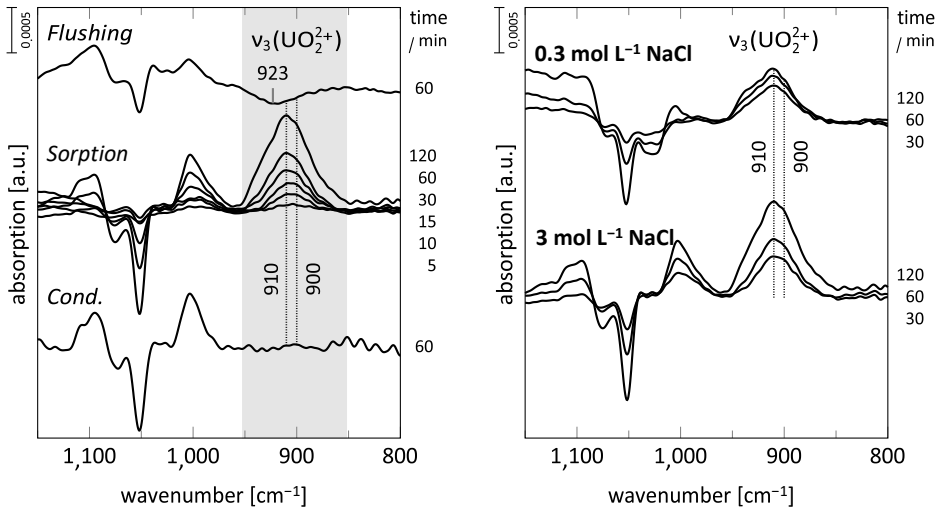

Fig. 4: *In situ* ATR FT-IR spectra of U(VI) sorption on montmorillonite in absence of CO_2 (D_2O, $c_{U(VI)} = 2 \times 10^{-5}$ mol L^{-1}, pH_c 6.8): Left: Experiment at 3 mol L^{-1} NaCl. Right: Comparison of U(VI) uptake at 0.3 mol L^{-1} and 3 mol L^{-1} NaCl. Here only sorption spectra are shown. (The spectra of the sorption process were recorded at different times after induction as indicated on the right-hand side of the plot. Ordinate scaling is given by the bar in units of optical density. Other values indicated are in cm^{-1}.)

During the U(VI) sorption process onto montmorillonite, a very broad band of ν_3 emerges with a maximum at 910 cm^{-1}, with a distinct shoulder at 900 cm^{-1} possibly indicating the presence of more than one surface species. The shift of more than 10 cm^{-1} in comparison to the predicted species in solution points to the formation of an inner-sphere uranyl complex on the montmorillonite surface. The *in situ* vibrational data of U(VI) sorbed onto other oxides of Al and Ti serving as references show similar shifts of the ν_3 mode under identical U(VI) concentrations (Müller et al., 2013; Müller et al., 2012). A coordination of the actinyl ion by outer-sphere complexation (electrostatic attraction) is not expected to shift the absorption frequency to such an extent (Lefèvre, 2004). No further changes in the spectra are observed after prolonged sorption (120 min), indicating that the montmorillonite film is saturated with U(VI).

In the spectrum of the flushing stage (Fig. 4, left, upper trace), the absence of a negative band of ν_3 around 910 cm^{-1} indicates that none of the sorbed species were easily removed by flushing the mineral with the blank solution. This strengthens the assumption of the formation of an inner-sphere sorption complex. The very small negative band located at 923 cm^{-1} can be explained by flushing of remaining aqueous complexes from the pores of the mineral film.

In order to check the impact of ionic strength on the U(VI) sorption complex, the experiment was repeated using a 0.3 mol L^{-1} NaCl solution as background electrolyte. A comparison of the calculated ATR FT-IR difference spectra of the sorption stage is shown in Fig. 4 (right). The position of the spectral signal seems to

be identical, indicating the formation of equal sorption complexes. However, the intensity of the ν_3 related band at 910 cm^{-1} is found to be slightly lower. This confirms the result of the batch sorption study, namely the slightly increase of the U(VI) sorption with ionic strength in NaCl at $pH_c \approx 7$. Experiments in 3 mol L^{-1} NaCl in presence of CO_2 and in 1 mol L^{-1} $CaCl_2$ showed a signal-noise ratio that prevented meaningful interpretation of the spectra.

As shown by ATR FT-IR spectroscopy, U(VI) speciation on the clay surface was mostly identical for low and high ionic strength under the applied experimental conditions. Schnurr et al. (2015) have made similar observations for Eu(III) and Cm(III) sorption to clay minerals. SCM in the present study was therefore conducted under the assumption that the processes responsible for U(VI) uptake are the same at low and high ionic strengths.

3.4. Surface complexation modeling and parameter derivation

To derive surface complexation constants (log $K°$ values) for the U(VI) sorption onto montmorillonite all experimental sorption data discussed in Section 2.4 (cf. Table S2 in SI) were fitted simultaneously. The proposed surface species based on the evidence provided by previous spectroscopic studies and published works. This choice replicates the most important patterns of the aqueous U(VI) speciation in a simplified version, i.e. U(VI) hydroxide complexes were assumed to be present on the clay mineral surface under conditions in which U(VI) hydroxides dominate the aqueous U(VI) speciation. We assumed monodentate surface complexes only to be as much as possible consistent to the original 2SPNE SC/CE application for this system in Marques Fernandes et al. (2012). Moreover, only strong sites were considered as mentioned in Section 2.4 due to the experimental conditions of the sorption studies and the available sorption site capacity. The surface site capacities and protolysis constants for montmorillonite derived by Bradbury and Baeyens (1997) as well as the parameter of the CE reaction published by Bradbury and Baeyens (1995) and Bradbury and Baeyens (2005) were used as non-adjustable parameters as given in Table 1 (cf. Section 2.4). As mentioned in Section 3.2, CE decreases with increasing ionic strength and only plays a role below pH 4. Keeping all this in mind, the only adjustable parameters were the stability constants for surface complexation reactions on strong sites for fitting the experimental sorption data.

The modeling procedure was carried out stepwise. Based on the original parameters as described in Bradbury and Baeyens (2005) as well as in Marques Fernandes et al. (2012) (cf. Table S8 in SI), the surface complexation reactions for the surface complexes on the strong sites were considered. However, it is expected

that the adsorption of carbonate species on the negatively charged montmorillonite can be neglected as described similarly for negatively charged feldspars (Neumann et al., 2021) or quartz (Vuceta, 1976). Tournassat et al. (2018) described that the U(VI) sorption on montmorillonite under real atmospheric conditions can be modeled without the formation of uranyl carbonate surface complexes (U-CO_3-complexes). This was also attempted by Marques Fernandes et al. (2012). Thus, a SCM model without (SCM-A) and with a ternary U-CO_3-surface complex (SCM-B) was developed to fit the data in this work. The surface complex $\equiv S^SOUO_2(OH)_2^-$ occurs between $\equiv S^SOUO_2OH$ and $\equiv S^SOUO_2(OH)_3^{2-}$ as described in Marques Fernandes et al. (2012) and the inclusion of this complex in the set of surface complexes led to higher standard deviations of the final log $K°$ values and the overall error CEV (cf. Section 2.4). Therefore, this surface complex $\equiv S^SOUO_2(OH)_2^-$ was excluded from the set of surface species. This leaves the surface complexes $\equiv S^SOUO_2^+$, $\equiv S^SOUO_2OH$, and $\equiv S^SOUO_2(OH)_3^{2-}$ for SCM-A to describe U(VI) surface complexation on montmorillonite (cf. Table 2). For SCM-B the surface complexes $\equiv S^SOUO_2^+$, $\equiv S^SOUO_2OH$, $\equiv S^SOUO_2(OH)_3^{2-}$, and $\equiv S^SOUO_2(CO_3)_2^{3-}$ were considered (cf. Table S8 in SI). The surface complex $\equiv S^SOUO_2CO_3^-$ is expected to influence U(VI) sorption in nearly the same pH_c range as the surface complex $\equiv S^SOUO_2OH$ and is therefore excluded from the set of surface species. The reduction of the number of parameters renders the model more robust and avoids insignificant species or species where stability constants are highly correlated. Here, it should be mentioned, that such a reduced set of the surface complexes might be too restrictive when expanding the boundary conditions well beyond the limits of this work. The results show that no ternary U-CO_3-surface complex is required to fit the data. The surface complexation reactions for the considered U(VI) surface complexes and the fitted log $K°$ values of the SCM-A model are given in Table 2. The standard deviation for the log $K°$ values and the resulting CEV of 89 are taken from the UCODE output file. The dependence of the individual model parameters was checked using the correlation matrix calculated by UCODE as part of the fit procedure. Due to the given chemical correlations (same type of reactions, hydrolysis of the surface complexes), the log $K°$ values of the surface complexation reactions show some minor correlation and are not completely independent of each other. However, with correlation coefficients of < 0.3, only weak interdependence is indicated (cf. Table S9 in SI).

Table 2: Surface complexation reactions and log $K°$ values derived in the present work, errors correspond to ± 2σ. Abbreviations for the surface complexes (SC) are used in Figs. 5, 6, S4, S8, S11 and S12.

	Surface complexation reactions	log $K°$
SC-1	$\equiv S^SOH + UO_2^{2+} \rightleftharpoons \equiv S^SOUO_2^+ + H^+$	2.42 ± 0.04
SC-2	$\equiv S^SOH + UO_2^{2+} + H_2O \rightleftharpoons \equiv S^SOUO_2OH + 2\ H^+$	−4.49 ± 0.7
SC-3	$\equiv S^SOH + UO_2^{2+} + 3\ H_2O \rightleftharpoons \equiv S^SOUO_2(OH)_3^{2-} + 4\ H^+$	−20.5 ± 0.4

Figs. 3 and 5 show the SCM results obtained by applying the above SCM-A model. Obviously, the experimental data can be satisfactorily reproduced with this model at all the different experimental conditions.

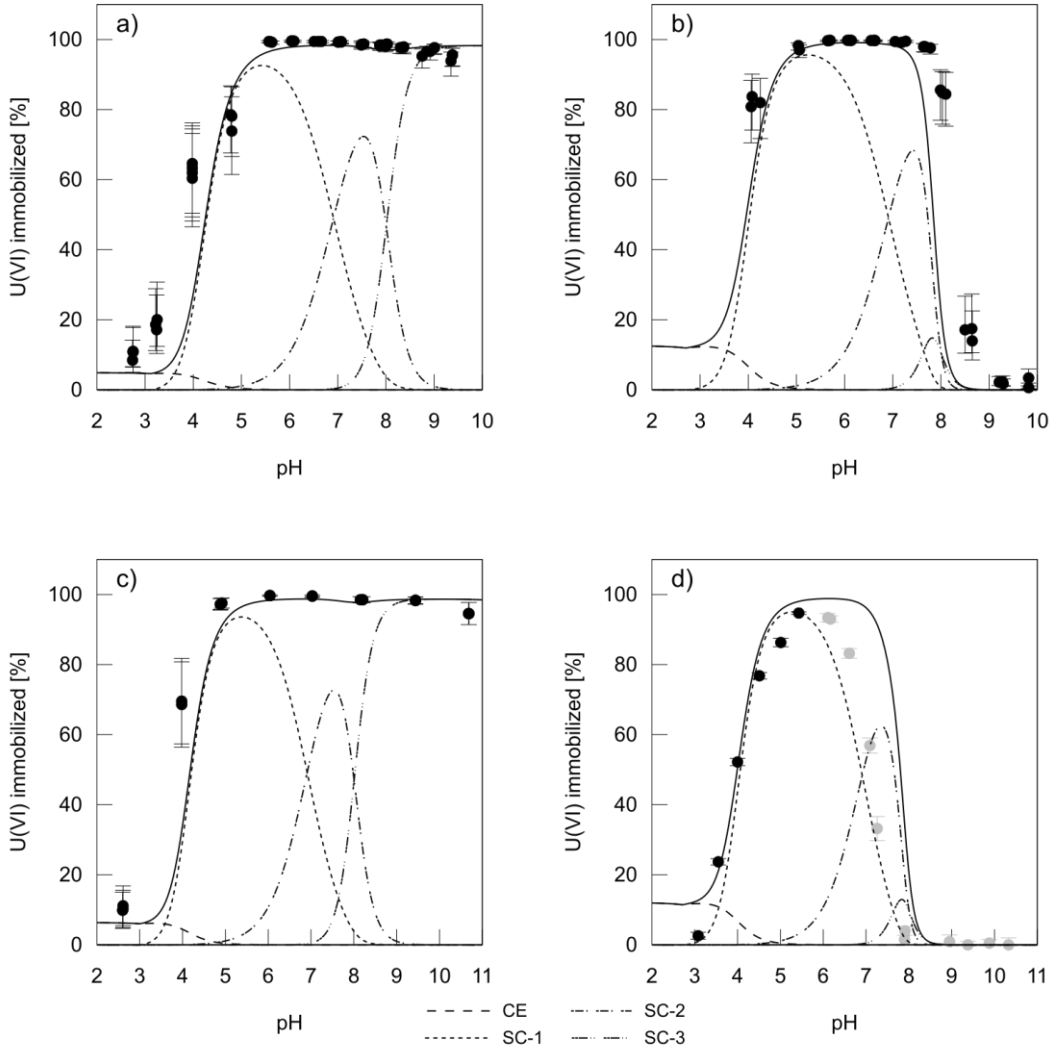

Fig. 5: U(VI) experimental batch sorption data for montmorillonite (symbols) and simulated results using the SCM model without ternary U-CO_3-surface complex (SCM-A) (lines) from different studies: (a) Marques Fernandes et al. (2012) ($c_{U(VI)} = 9 \times 10^{-8}$ mol L^{-1}, I = 0.1 mol L^{-1} $NaClO_4$, in absence of CO_2), (b) Marques Fernandes et al. (2012) ($c_{U(VI)} = 9 \times 10^{-8}$ mol L^{-1}, I = 0.1 mol L^{-1} $NaClO_4$, in presence of CO_2 ($p_{CO_2} = 10^{-3.5}$ atm), (c) Bradbury and Baeyens (2005) ($c_{U(VI)} = 1.4 \times 10^{-7}$ mol L^{-1}, I = 0.1 mol L^{-1} $NaClO_4$, in absence of CO_2), (d) Nebelung et al. (2007) ($c_{U(VI)} = 1 \times 10^{-6}$ mol L^{-1}, I = 0.1 mol L^{-1} $NaClO_4$, in presence of CO_2 ($p_{CO_2} = 10^{-3.5}$ atm). Designation of surface complexes SC-1 to SC-3 cf. Table 2. (Marked with grey dots: Outlier as explained in Section 2.4).

The comparison with the surface complexation constants reported by Bradbury and Baeyens (2005) and Marques Fernandes et al. (2012) (cf. Table S8 in SI) shows that the constants derived in the present work are rather close to the parameters given in the aforementioned publications. Up to pH 6-7, the U(VI) sorption is approximately the same in carbonate-containing and carbonate-free systems as well as for both background electrolytes. In the $NaCl/NaClO_4$ systems a complete U(VI) sorption occurs above pH_c 6 in the absence of carbonate. In the presence of carbonate, the sorption maximum is between pH_c 6 and 7.5 and a significant decrease in the U(VI) retention can be seen above pH_c 7.5 down to nearly zero % sorption at pH 9 due to the formation of aqueous U(VI) carbonate complexes. Here, the difference of the experimental sorption data of Nebelung et al. (2007) at $pH_c > 6$ to the data of the present work and of Marques Fernandes et al. (2012) as described in Section 2.4 can be seen and explain the deviation of the modeled sorption edge of Nebelung et al. (2007) in the alkaline pH range. As can be seen in Figs. 3 and 5 no ternary U-CO_3-surface complex is required to fit the data and four parameters (three binary surface complexation reactions and the CE reaction) are sufficient to describe the sorption edges of the U(VI)-montmorillonite system. However, the results of SCM-B with ternary U-CO_3-surface complex (cf. Figs. S7 and S8 in SI) are still comparable to SCM-A, which indicates the low relevance of the U-CO_3-surface complex. However, a slight underestimation of the experimental data of Marques Fernandes et al. (2012) in the presence of carbonate can be seen with SCM-A at pH > 7 (cf. Fig. 5b), which is acceptable due to the high error bars. With SCM-B the data at pH > 7 of Marques Fernandes et al. (2012) (cf. Fig. S8b in SI) are somewhat more accurately described but overestimate the sorption edges in the alkaline pH range of comparable systems as described in Section 3.4.1 (cf. Fig. 6). As the objective of this work was to develop a robust and comprehensive model for U(VI) sorption onto montmorillonite we prefer the SCM-A model without ternary U-CO_3-surface complex as already recommended by Tournassat et al. (2018). Thus, U(VI) sorption on montmorillonite at various ionic strengths, which is almost completely governed by U(VI) surface complexation, can be well described.

3.4.1. Validation of the final SCM model

To validate the developed SCM model, we compared U(VI) batch sorption results on montmorillonite published by Pabalan et al. (1998) ($c_{U(VI)}$: 2.45×10^{-7} mol L^{-1}, pH: 2 - 9, I: 0.1 mol L^{-1} $NaNO_3$, SLR: 3.2 g kg_{water}^{-1}, SSA: 97 m^2 g^{-1}) to predictions computed with our SCM set of species and the associated log $K°$ values derived in the present study (cf. Table 2 for SCM-A and in SI Table S8 for SCM-B), as well as the values for surface protolysis and binding site densities (cf. Table 1). As can be seen in Fig. 6 and Fig. S11 in

SI, the SCM-A without a ternary U-CO_3-surface complex provides simulations in excellent agreement with the experimental data published by Pabalan et al. (1998).

It can be observed that the U(VI) retention is dominated by the surface complex $\equiv S^SOUO_2^+$ (SC-1), followed by the $\equiv S^SOUO_2OH$ (SC-2), and $\equiv S^SOUO_2(OH)_3^{2-}$ (SC-3). Below pH 3.5, U(VI) is sorbing primarily to cation exchange sites. At pH > 3.5, an increased U(VI) retention is observed caused by pH-dependent surface complexation reactions due to the enhanced deprotonation of the surface sites. The sorption maximum is between pH 5.5 and 7. Above pH 7, a significant decrease of the U(VI) retention can be seen down to nearly zero % sorption at pH 9, comparable to the experimental data of the present work and of Marques Fernandes et al. (2012) (cf. Figs. 3 and 5). This is due to the formation of aqueous U(VI) carbonate complexes in the alkaline pH range. The ternary U-CO_3-surface complex $\equiv S^SOUO_2(CO_3)_2^{3-}$ (SC-4) is not required to simulate the U(VI) retention above pH 7.5. As can be seen in Fig. S12 in SI, the inclusion of this complex leads to an overestimation of the U(VI) sorption at alkaline conditions.

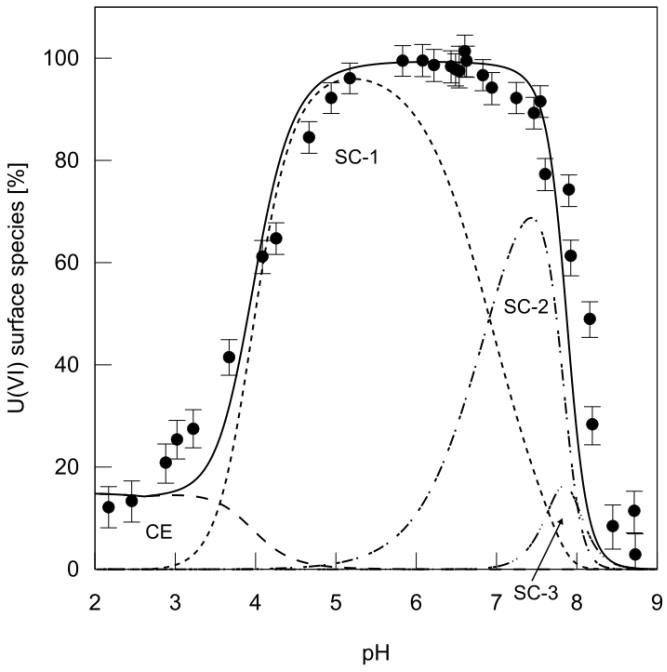

Fig. 6: U(VI) experimental batch sorption data for montmorillonite from Pabalan et al. (1998) (symbols) ($c_{U(VI)}$ = 2.45 × 10^{-7} mol L^{-1}, I = 0.1 mol L^{-1} $NaNO_3$, in presence of CO_2 (p_{CO_2} = $10^{-3.5}$ atm) and predictive modeling results (lines) using the final SCM model without ternary U-CO_3-surface complex (SCM-A) of this study. Designation of surface complexes SC-1 to SC-3 cf. Table 2.

These simulations show that the predictive modeling using the SCM-A model as a simplified version of the 2SPNE SC/CE model yields results that compare well with the U(VI) sorption data reported in the open literature, demonstrating the robustness of the developed SCM.

4. Conclusions

New insights into the U(VI) sorption on the clay mineral montmorillonite at increased ionic strength were obtained, using a multi-method approach combining batch sorption experiments with spectroscopic methods (TRLFS, ATR FT-IR) as well as SCM. These investigations focused on a wide range of experimental conditions: absence and presence of CO_2, variation of pH_c, background electrolytes (NaCl and $CaCl_2$) and ionic strength (up to 3 mol kg^{-1}).

In the absence of carbonate, U(VI) was almost quantitatively sorbed (nearly 99%) above pH_c 6 in both NaCl and $CaCl_2$ due to deprotonation of surface sites. No significant ionic strength effect was observed. Below pH_c 4 and at low ionic strengths, U(VI) is bound primarily to cation exchange sites in the interlayer. With increasing ionic strength, cation exchange is strongly reduced, in particular in the NaCl system. However, if the differences in ionic strength stay within one order of magnitude, the differences in U(VI) uptake are small (< 1%).

In the presence of carbonate, U(VI) sorption was reduced above pH_c 7.5 in the NaCl system because of aqueous U(VI) carbonate complexes. In the $CaCl_2$ system, U(VI) sorption is strongly reduced between pH_c 6 and 7 due to formation of the neutral $Ca_2UO_2(CO_3)_{3(aq)}$ complex in aqueous solution, as confirmed by TRLFS in accordance with thermodynamic modeling. A significant ionic strength effect is observed here, caused by the formation of the thermodynamically stable, neutral $Ca_2UO_2(CO_3)_{3(aq)}$ complex, which forms at lower pH values as Ca concentration and ionic strength increase. Under alkaline conditions, the U(VI) retention increases again due to the precipitation of calcite ($CaCO_3$). As a result, the carbonate content and thus, the amount of uranyl carbonate complexes in solution is reduced at laboratory conditions. However, in a deep geological disposal setting, re-adsorption of carbonate in solution can be expected as a long-term effect.

Based on the batch sorption and spectroscopic data from this study, as well as from published U(VI) sorption studies on montmorillonite conducted under somewhat different experimental conditions, a robust and comprehensive surface complexation model, based on the 2SPNE SC/CE model of Bradbury and Baeyens (1997), was developed. It successfully describes the experimental data at various ionic strengths in the absence and presence of carbonates by considering only strong sorption sites. It was confirmed that ternary uranyl

carbonate surface complexes are not required to model the U(VI) sorption onto montmorillonite under atmospheric conditions as previously suggested by Tournassat et al. (2018). Four reaction parameters (three binary surface complexation reactions and the CE reaction) are sufficient to model the U(VI) sorption edges (at trace U concentrations) for different geochemical conditions. This is an improvement compared to the up to ten parameters previously used by Marques Fernandes et al. (2012), where in addition isotherms in the absence and presence of carbonate were considered. However, it should be noted, too, that the 2SPNE SC/CE model clearly reaches its limits of applicability at high ionic strengths, as can be seen especially for the high ionic strength data points in the pH range 5 to 6.

The obtained surface complexation constants (log $K°$ values) are substantial for a realistic geochemical modeling of U(VI) transport in groundwaters. In particular, the obtained stability constants will extend the thermodynamic database for the smart K_d-concept (Stockmann et al., 2017), as a modern approach to simulate the radionuclide transport for a wide range of geochemical conditions. As the K_d paradigm is still the most often encountered approach in environmental chemistry and geochemistry, the results of this study have also been converted into K_d-based graphs that are compiled in SI.

With respect to the long-term safety assessment of a radioactive waste repository in argillaceous rock at elevated salinity levels, the results demonstrate that increased ionic strengths up to 3 mol kg^{-1} have no significant effect at environmentally relevant pH conditions. This is different in the presence of calcium, since uranium(VI) sorption is then restrained by the preferential formation of the $Ca_2UO_2(CO_3)_{3(aq)}$ complex with increasing calcium concentration and thus increasing ionic strength. Predictive modeling of U(VI) sorption processes in complex clay rich natural environments should take this into account for safety assessments.

CRediT authorship contribution statement

M. Stockmann: Methodology, Validation, Writing - review & editing. **K. Fritsch:** Investigation, Formal analysis, Writing - original draft. **F. Bok:** Methodology. **M. Marques Fernandes:** Writing - review & editing. **B. Baeyens:** Writing - review & editing. **R. Steudtner:** Investigation. **K. Müller:** Investigation, Writing - review & editing. **C. Nebelung:** Investigation. **V. Brendler:** Methodology, Writing - review & editing. **T. Stumpf:** Writing - review & editing, Funding acquisition, Supervision. **K. Schmeide:** Conceptualization, Writing - review & editing, Funding acquisition, Supervision.

Acknowledgements

The authors would like to thank S. Gürtler for work on several sample series, A. Chlupka, C. Müller, S. Schubert, S. Beutner and C. Eckardt for ICP-MS, AAS, ion chromatography and BET measurements, A. Scholz for XRD measurements and K. Heim for ATR FT-IR measurements.

Funding

This work was supported by the German Federal Ministry for Economic Affairs and Energy (BMWi) through the GRaZ II project (grants 02E10971 and 02E11860B) and by the German Federal Ministry of Education and Research (BMBF) (grant 02NUK053B) and the Helmholtz Association (grant SO-093) through the iCross project.

Supplementary Material

Supplementary material to this article can be found in the appendix.

References

Abend, S., Lagaly, G., 2000. Sol-gel transitions of sodium montmorillonite dispersions. Appl. Clay Sci. 16, 201-227.

Al-Masri, M.S., Nashawati, A., Amin, Y., Al-Masri, W., Al-Howary, M.A., 2019. Comparison of U-238, Po-210 and Pb-210 speciation in six different types of soils. Bull. Environ. Contam. Toxicol. 102, 239-245.

Altmaier, M., Metz, V., Neck, V., Müller, R., Fanghänel, T., 2003. Solid-liquid equilibria of $Mg(OH)_{2(cr)}$ and $Mg_2(OH)_3Cl{\cdot}4H_2O_{(cr)}$ in the system Mg-Na-H-OH-Cl-H_2O at 25°C. Geochim. Cosmochim. Acta 67, 3595-3601.

Altmaier, M., Neck, V., Fanghänel, T., 2008. Solubility of Zr(IV), Th(IV) and Pu(IV) hydrous oxides in $CaCl_2$ solutions and the formation of ternary Ca-M(IV)-OH complexes. Radiochim. Acta 96, 541-550.

Amayri, S., Fröhlich, D.R., Kaplan, U., Trautmann, N., Reich, T., 2016. Distribution coefficients for the sorption of Th, U, Np, Pu, and Am on Opalinus Clay. Radiochim. Acta 104, 33-40.

Ams, D.A., Swanson, J.S., Szymanowski, J.E.S., Fein, J.B., Richmann, M., Reed, D.T., 2013. The effect of high ionic strength on neptunium(V) adsorption to a halophilic bacterium. Geochim. Cosmochim. Acta 110, 45-57.

ANDRA, 2005. Dossier 2005 Argile - Synthesis, Evaluation of the feasibility of a geological repository in an argillaceous formation. Meuse/Haute-Marne site. ANDRA editor report series, Châtenay-Malabry Cedex, France.

Baeyens, B., Bradbury, M.H., 1997. A mechanistic description of Ni and Zn sorption on Na-montmorillonite. 1. Titration and sorption measurements. J. Contam. Hydrol. 27, 199-222.

Banik, N.L., Marsac, R., Lützenkirchen, J., Diascorn, A., Bender, K., Marquardt, C.M., Geckeis, H., 2016. Sorption and redox speciation of plutonium at the illite surface. Environ. Sci. Technol. 50, 2092-2098.

Bock, H., Dehandschutter, B., Martin, C.D., Mazurek, M., de Haller, A., Skoczylas, F., Davy, C., 2010. Self-sealing of Fractures in Argillaceous Formations in the Context of Geological Disposal of Radioactive Waste – Review and Synthesis. OECD/NEA, Issy-les-Moulineaux, France.

Bradbury, M.H., Baeyens, B., 1995. A quantitative mechanistic description of Ni, Zn and Ca sorption on Na-montmorillonite. Part III: Modelling. PSI Bericht Nr. 95-12, Switzerland.

Bradbury, M.H., Baeyens, B., 1997. A mechanistic description of Ni and Zn sorption on Na-montmorillonite. Part II: Modelling. J. Contam. Hydrol. 27, 223-248.

Bradbury, M.H., Baeyens, B., 1999. Modelling the sorption of Zn and Ni on Ca-montmorillonite. Geochim. Cosmochim. Acta 63, 325-336.

Bradbury, M.H., Baeyens, B., 2002. Sorption of Eu on Na- and Ca-montmorillonites: Experimental investigations and modelling with cation exchange and surface complexation. Geochim. Cosmochim. Acta 66, 2325-2334.

Bradbury, M.H., Baeyens, B., 2005. Modelling the sorption of Mn(II), Co(II), Ni(II), Zn(II), Cd(II), Eu(III), Am(III), Sn(IV), Th(IV), Np(V) and U(VI) on montmorillonite: Linear free energy relationships and estimates of surface binding constants for some selected heavy metals and actinides. Geochim. Cosmochim. Acta 69, 875-892.

Bradbury, M.H., Baeyens, B., 2006. Modelling sorption data for the actinides Am(III), Np(V) and Pa(V) on montmorillonite. Radiochim. Acta 94, 619-625.

Bradbury, M.H., Baeyens, B., 2009. Sorption modelling on illite. Part II: Actinide sorption and linear free energy relationships. Geochim. Cosmochim. Acta 73, 1004-1013.

Bradbury, M.H., Baeyens, B., Geckeis, H., Rabung, T., 2005. Sorption of Eu(III)/Cm(III) on Ca-montmorillonite and Na-illite. Part 2: Surface complexation modelling. Geochim. Cosmochim. Acta 69, 5403-5412.

Brewitz, W., 1982. Eignungsprüfung der Schachtanlage Konrad für die Endlagerung radioaktiver Abfälle. GSF-T 136, Gesellschaft für Strahlen- und Umweltforschung, Neuherberg, Germany.

Bruggeman, C., Liu, D.J., Maes, N., 2010. Influence of Boom Clay organic matter on the adsorption of Eu^{3+} by illite - geochemical modelling using the component additivity approach. Radiochim. Acta 98, 597-605.

Cao, X.Y., Zheng, L.G., Hou, D.Y., O'Connor, D., Hu, L.T., Wu, J., 2020. Modeling the risk of U(VI) migration through an engineered barrier system at a proposed Chinese high-level radioactive waste repository. Sci. Total Environ. 707, 9.

Catalano, J.G., Brown, G.E., 2005. Uranyl adsorption onto montmorillonite: Evaluation of binding sites and carbonate complexation. Geochim. Cosmochim. Acta 69, 2995-3005.

Chang, H.S., Korshin, G.V., Wang, Z.M., Zachara, J.M., 2006. Adsorption of uranyl on gibbsite: A time-resolved laser-induced fluorescence spectroscopy study. Environ. Sci. Technol. 40, 1244-1249.

Chipera, S.J., Bish, D.L., 2001. Baseline studies of the clay minerals society source clays: Powder X-ray diffraction analyses. Clay Clay Miner. 49, 398-409.

Collins, R.N., Saito, T., Aoyagi, N., Payne, T.E., Kimura, T., Waite, T.D., 2011. Applications of time-resolved laser fluorescence spectroscopy to the environmental biogeochemistry of actinides. J. Environ. Qual. 40, 731-741.

Comarmond, M.J., Steudtner, R., Stockmann, M., Heim, K., Müller, K., Brendler, V., Payne, T.E., Foerstendorf, H., 2016. The sorption processes of U(VI) onto SiO_2 in the presence of phosphate: From binary surface species to precipitation. Environ. Sci. Technol. 50, 11610-11618.

De Craen, M., Wang, L., Van Geet, M., Moors, H., 2004. Geochemistry of Boom Clay pore water at the Mol site. Scientific Report of the Belgian Nuclear Research Centre SCK•CEN-BLG-990, SCK•CEN, Mol, Belgium.

Dong, W.M., Ball, W.P., Liu, C.X., Wang, Z.M., Stone, A.T., Bai, J., Zachara, J.M., 2005. Influence of calcite and dissolved calcium on uranium(VI) sorption to a Hanford subsurface sediment. Environ. Sci. Technol. 39, 7949-7955.

Drobot, B., Steudtner, R., Raff, J., Geipel, G., Brendler, V., Tsushima, S., 2015. Combining luminescence spectroscopy, parallel factor analysis and quantum chemistry to reveal metal speciation - a case study of uranyl(VI) hydrolysis. Chem. Sci. 6, 964-972.

Fralova, L., Lefevre, G., Made, B., Marsac, R., Thory, E., Dagnelie, R.V.H., 2021. Effect of organic compounds on the retention of radionuclides in clay rocks: Mechanisms and specificities of Eu(III), Th(IV), and U(VI). Appl. Geochem. 127, 104859.

Ghayaza, M., Le Forestier, L., Muller, F., Tournassat, C., Beny, J.M., 2011. Pb(II) and Zn(II) adsorption onto Na- and Ca-montmorillonites in acetic acid/acetate medium: Experimental approach and geochemical modeling. J. Colloid Interf. Sci. 361, 238-246.

Giffaut, E., Grivé, M., Blanc, P., Vieillard, P., Colàs, E., Gailhanou, H., Gaboreau, S., Marty, N., Madé, B., Duro, L., 2014. ANDRA thermodynamic database for performance assessment: ThermoChimie. Appl. Geochem. 49, 225-236.

Glaus, M.A., Frick, S., Van Loon, L.R., 2020. A coherent approach for cation surface diffusion in clay minerals and cation sorption models: Diffusion of Cs^{+} and Eu^{3+} in compacted illite as case examples. Geochim. Cosmochim. Acta 274, 79-96.

Gorman-Lewis, D., Fein, J.B., Burns, P.C., 2008. Solubility measurements of the uranyl oxide hydrate phases metaschoepite, compreignacite, Na–compreignacite, becquerelite, and clarkeite. J. Chem. Thermodyn. 40, 980-990.

Götz, C., Geipel, G., Bernhard, G., 2011. The influence of the temperature on the carbonate complexation of uranium(VI): a spectroscopic study. J. Radioanal. Nucl. Chem. 287, 961-969.

Grambow, B., Fattahi, M., Montavon, G., Moisan, C., Giffaut, E., 2006. Sorption of Cs, Ni, Pb, Eu(III), Am(III), Cm, Ac(III), Tc(IV), Th, Zr, and U(IV) on MX 80 bentonite: An experimental approach to assess model uncertainty. Radiochim. Acta 94, 627-636.

Grenthe, I., Gaona, X., Plyasunov, A.V., Rao, L., Runde, W.H., Grambow, B., Konings, R.J.M., Smith, A.L., Moore, E.E., 2020. Second Update on the Chemical Thermodynamics of Uranium, Neptunium, Plutonium, Americium and Technetium. Chemical Thermodynamics 14. OECD Nuclear Energy Agency Data Bank, Eds., OECD Publications, Boulogne-Billancourt, France.

Grim, R.E., 1968. Clay mineralogy. 596 p, New York (Mc Graw-Hill).

Guggenheim, E.A., Turgeon, J.C., 1955. Specific interaction of ions. Trans. Faraday Soc. 51, 747-761.

Guillaumont, R., Fanghänel, T., Neck, V., Fuger, J., Palmer, D.A., Grenthe, I., Rand, M.H., 2003. Update on the Chemical Thermodynamics of Uranium, Neptunium, Plutonium, Americium and Technetium. Volume 5. OECD Nuclear Energy Agency Data Bank, Eds., North Holland Elsevier Science Publishers B. V., Amsterdam, The Netherlands.

Hama, K., Kunimaru, T., Metcalfe, R., Martin, A.J., 2007. The hydrogeochemistry of argillaceous rock formations at the Horonobe URL site, Japan. Phys. Chem. Earth 32, 170-180.

Hartmann, E., Geckeis, H., Rabung, T., Lützenkirchen, J., Fanghänel, T., 2008. Sorption of radionuclides onto natural clay rocks. Radiochim. Acta 96, 699-707.

Hennig, T., Stockmann, M., Kühn, M., 2020. Simulation of diffusive uranium transport and sorption processes in the Opalinus Clay. Appl. Geochem. 123, 104777.

Hoth, P., Wirth, H., Reinhold, K., Bräuer, V., Krull, P., Feldrappe, H., 2007. Final disposal of radioactive wastes in deep geological formations of Germany. Investigation and evaluation of argillaceous rock formations. Bundesanstalt für Geowissenschaften und Rohstoffe (BGR), Berlin/Hannover, Germany.

IAEA, 2003. Extent of environmental contamination by naturally occurring radioactive material (NORM) and technological options for mitigation. Technical reports series No. 419, IAEA, Vienna, Austria.

Joseph, C., Mibus, J., Trepte, P., Muller, C., Brendler, V., Park, D.M., Jiao, Y.Q., Kersting, A.B., Zavarin, M., 2017. Long-term diffusion of U(VI) in bentonite: Dependence on density. Sci. Total Environ. 575, 207-218.

Joseph, C., Stockmann, M., Schmeide, K., Sachs, S., Brendler, V., Bernhard, G., 2013a. Sorption of U(VI) onto Opalinus Clay: Effects of pH and humic acid. Appl. Geochem. 36, 104-117.

Joseph, C., Van Loon, L.R., Jakob, A., Steudtner, R., Schmeide, K., Sachs, S., Bernhard, G., 2013b. Diffusion of U(VI) in Opalinus Clay: Influence of temperature and humic acid. Geochim. Cosmochim. Acta 109, 74-89.

Křepelová, A., Brendler, V., Sachs, S., Baumann, N., Bernhard, G., 2007. U(VI)-kaolinite surface complexation in absence and presence of humic acid studied by TRLFS. Environ. Sci. Technol. 41, 6142-6147.

Lefèvre, G., 2004. In situ Fourier-transform infrared spectroscopy studies of inorganic ions adsorption on metal oxides and hydroxides. Adv. Colloid Interface Sci. 107, 109-123.

Marques Fernandes, M., Baeyens, B., 2020. Competitive adsorption on illite and montmorillonite: Experimental and modelling investigations. Nagra Technical Report, NTB 19-05, Nagra, Wettingen, Switzerland.

Marques Fernandes, M., Baeyens, B., Dähn, R., Scheinost, A.C., Bradbury, M.H., 2012. U(VI) sorption on montmorillonite in the absence and presence of carbonate: A macroscopic and microscopic study. Geochim. Cosmochim. Acta 93, 262-277.

Marques Fernandes, M., Scheinost, A.C., Baeyens, B., 2016. Sorption of trivalent lanthanides and actinides onto montmorillonite: Macroscopic, thermodynamic and structural evidence for ternary hydroxo and carbonato surface complexes on multiple sorption sites. Water Res. 99, 74-82.

Marsac, R., Banik, N.L., Lützenkirchen, J., Diascorn, A., Bender, K., Marquardt, C.M., Geckeis, H., 2017. Sorption and redox speciation of plutonium at the illite surface under highly saline conditions. J. Colloid Interf. Sci. 485, 59-64.

Mazurek, M., 2004. Long-term used nuclear fuel waste management – Geoscientific review of the sedimentary sequence in southern Ontario. Technical Report TR 0401, Institute of Geological Sciences, University of Bern, Bern, Switzerland.

Meleshyn, A., Azeroual, M., Reeck, T., Houben, G., Riebe, B., Bunnenberg, C., 2009. Influence of (calcium-)uranyl-carbonate complexation on U(VI) sorption on Ca- and Na-bentonites. Environ. Sci. Technol. 43, 4896-4901.

Missana, T., Garcia-Gutierrez, M., 2007. Adsorption of bivalent ions (Ca(II), Sr(II) and Co(II)) onto FEBEX bentonite. Phys. Chem. Earth 32, 559-567.

Morse, J.W., Arvidson, R.S., Lüttge, A., 2007. Calcium carbonate formation and dissolution. Chem. Rev. 107, 342–391.

Moulin, C., Laszak, I., Moulin, V., Tondre, C., 1998. Time-resolved laser-induced fluorescence as a unique tool for low-level uranium speciation. Appl. Spectrosc. 52, 528-535.

Müller, K., Brendler, V., Foerstendorf, H., 2008. Aqueous uranium(VI) hydrolysis species characterized by attenuated total reflection Fourier-transform infrared spectroscopy. Inorg. Chem. 47, 10127-10134.

Müller, K., Foerstendorf, H., Brendler, V., Rossberg, A., Stolze, K., Gröschel, A., 2013. The surface reactions of U(VI) on γ-Al_2O_3 - In situ spectroscopic evaluation of the transition from sorption complexation to surface precipitation. Chem. Geol. 357, 75-84.

Müller, K., Foerstendorf, H., Meusel, T., Brendler, V., Lefèvre, G., Comarmond, M.J., Payne, T.E., 2012. Sorption of U(VI) at the TiO_2-water interface: An in situ vibrational spectroscopic study. Geochim. Cosmochim. Acta 76, 191-205.

Nagasaki, S., Saito, T., Yang, T.T., 2016. Sorption behavior of Np(V) on illite, shale and MX-80 in high ionic strength solutions. J. Radioanal. Nucl. Chem. 308, 143-153.

Nagra, 2002. Project Opalinus Clay. Safety report. Demonstration of disposal feasibility for spent fuel, vitrified high-level waste and long-lived intermediate-level waste. NTB 02-05, Nagra, Wettingen, Switzerland.

Nebelung, C., Brendler, V., Křepelová, A., Brockmann, S., 2007. Sorption of uranium and caesium on bentonite, experiments and modelling. WP2.5: Radionuclide transport (sorption and diffusion) in the clay engineered barrier and sorption onto corrosion products (D2.5.15), NF-PRO Report.

Neumann, J., Brinkmann, H., Britz, S., Lutzenkirchen, J., Bok, F., Stockmann, M., Brendler, V., Stumpf, T., Schmidt, M., 2021. A comprehensive study of the sorption mechanism and thermodynamics of f-element sorption onto K-feldspar. J. Colloid Interface Sci. 591, 490-499.

OECD/NEA, 2012. Thermodynamic Sorption Modelling in Support of Radioactive Waste Disposal Safety Cases: NEA Sorption Project Phase III. OECD Publishing, Paris, https://doi.org/10.1787/9789264177826-en.

Ojovan, M.I., Lee, W.E., 2005. An introduction to nuclear waste immobilisation, 1st Edition. Elsevier, Amsterdam, Netherlands.

ONDRAF/NIRAS, 2013. ONDRAF/NIRAS Research, Development and Demonstration (RD&D) Plan for the geological disposal of high-level and/or long-lived radioactive waste including irradiated fuel if considered as waste, State-of-the-art report as of December 2012, ONDRAF/NIRAS, Report NIROND-TR 2013-12 E, Brussels, Belgium.

Pabalan, R.T., Turner, D.R., 1997. Uranium(6+) sorption on montmorillonite: Experimental and surface complexation modeling study. Aquat. Geochem. 2, 203-226.

Pabalan, R.T., Turner, D.R., Bertetti, F.P., Prikyl, J.D., 1998. Uranium(VI) sorption onto selected mineral surfaces. Key geochemical parameters. In: Adsorption of metals by geomedia. Variables, mechanisms, and model applications. Jenne E.A. (Ed.); Academic Press; San Diego.

Papastefanou, C., Manolopoulou, M., Stoulos, S., Ioannidou, A., Gerasopoulos, E., 2000. Characterization of a karstic system by examining the occurrence of radioactive nuclides and trace elements. Nuovo Cimento Soc. Ital. Fis. C-Geophys. Space Phys. 23, 411-421.

Parkhurst, D.L., Appelo, C.A.J., 2013. Description of input and examples for PHREEQC version 3—A computer program for speciation, batch-reaction, one-dimensional transport, and inverse geochemical calculations, U.S. Geological Survey Techniques and Methods, book 6, chap. A43, 497 p., available only at https://pubs.usgs.gov/tm/06/a43/.

Payne, T.E., Brendler, V., Ochs, M., Baeyens, B., Brown, P.L., Davis, J.A., Ekberg, C., Kulik, D.A., Lutzenkirchen, J., Missana, T., Tachi, Y., Van Loon, L.R., Altmann, S., 2013. Guidelines for thermodynamic sorption modelling in the context of radioactive waste disposal. Environ. Modell. Softw. 42, 143-156.

Pearson, F.J., Arcos, D., Bath, A., Boisson, J.-Y., Fernández, A.M., Gäbler, H.-E., Gaucher, E., Gautschi, A., Griffault, L., Hernan, P., Waber, H.N., 2003. Mont Terri Project – Geochemistry of water in the Opalinus Clay formation at the Mont Terri rock laboratory. Reports of the FOWG Geology Series 5, Federal Office for the Environment, Bern, Switzerland.

Philipp, T., Shams Aldin Azzam, S., Rossberg, A., Huittinen, N., Schmeide, K., Stumpf, T., 2019. U(VI) sorption on Ca-bentonite at (hyper)alkaline conditions - Spectroscopic investigations of retention mechanisms. Sci. Total Environ. 676, 469-481.

Poeter, E.P., Hill, M.C., Lu, D., Tiedeman, C., Mehl, S.W., 2014. UCODE_2014, with new capabilities to define parameters unique to predictions, calculate weights using simulated values, estimate parameters with SVD, evaluate uncertainty with MCMC, and more. Report GWMI 2014-02. Integrated Groundwater Modeling Center of the Colorado School of Mines.

Poetsch, M., Lippold, H., 2016. Effects of ionic strength and fulvic acid on adsorption of Tb(III) and Eu(III) onto clay. J. Contam. Hydrol. 192, 146-151.

Quilès, F., Burneau, A., 2000. Infrared and Raman spectra of uranyl(VI) oxo-hydroxo complexes in acid aqueous solutions: a chemometric study. Vib. Spectrosc. 23, 231-241.

Rabung, T., Pierret, M.C., Bauer, A., Geckeis, H., Bradbury, M.H., Baeyens, B., 2005. Sorption of Eu(III)/Cm(III) on Ca-montmorillonite and Na-illite. Part 1: Batch sorption and time-resolved laser fluorescence spectroscopy experiments. Geochim. Cosmochim. Acta 69, 5393-5402.

Richter, C., Müller, K., Drobot, B., Steudtner, R., Großmann, K., Stockmann, M., Brendler, V., 2016. Macroscopic and spectroscopic characterization of uranium(VI) sorption onto orthoclase and muscovite and the influence of competing Ca^{2+}. Geochim. Cosmochim. Acta 189, 143-157.

Schmeide, K., Bernhard, G., 2010. Sorption of Np(V) and Np(IV) onto kaolinite: Effects of pH, ionic strength, carbonate and humic acid. Appl. Geochem. 25, 1238-1247.

Schmeide, K., Gürtler, S., Müller, K., Steudtner, R., Joseph, C., Bok, F., Brendler, V., 2014. Interaction of U(VI) with Äspö diorite: A batch and in situ ATR FT-IR sorption study. Appl. Geochem. 49, 116-125.

Schnurr, A., Marsac, R., Rabung, T., Lützenkirchen, J., Geckeis, H., 2015. Sorption of Cm(III) and Eu(III) onto clay minerals under saline conditions: Batch adsorption, laser-fluorescence spectroscopy and modeling. Geochim. Cosmochim. Acta 151, 192-202.

Semenkova, A.S., Evsiunina, M.V., Verma, P.K., Mohapatra, P.K., Petrov, V.G., Seregina, I.F., Bolshov, M.A., Krupskaya, V.V., Romanchuk, A.Y., Kalmykov, S.N., 2018. Cs^{+} sorption onto Kutch clays: Influence of competing ions. Appl. Clay Sci. 166, 88-93.

Shang, C.M., Reiller, P.E., 2020. Determination of formation constants and specific ion interaction coefficients for $Ca_nUO_2(CO_3)_3^{(4-2n)-}$ complexes in NaCl solution by time-resolved laser-induced luminescence spectroscopy. Dalton Trans. 49, 466-481.

Sposito, G., 2008. The chemistry of soils. Oxford University Press. New York.

Steudtner, R., Arnold, T., Geipel, G., Bernhard, G., 2010. Fluorescence spectroscopic study on complexation of uranium(VI) by glucose: a comparison of room and low temperature measurements. J. Radioanal. Nucl. Chem. 284, 421-429.

Steudtner, R., Sachs, S., Schmeide, K., Brendler, V., Bernhard, G., 2011. Ternary uranium(VI) carbonato humate complex studied by cryo-TRLFS. Radiochim. Acta 99, 687-692.

Stockmann, M., Schikora, J., Becker, D.A., Flügge, J., Noseck, U., Brendler, V., 2017. Smart K_d-values, their uncertainties and sensitivities - Applying a new approach for realistic distribution coefficients in geochemical modeling of complex systems. Chemosphere 187, 277-285.

Sugiura, Y., Ishidera, T., Tachi, Y., 2021. Surface complexation of Ca and competitive sorption of divalent cations on montmorillonite under alkaline conditions. Appl. Clay Sci. 200, 105910.

Szymanek, K., Charmas, R., Piasecki, W., 2021. Investigations of mechanism of Ca^{2+} adsorption on silica and alumina based on Ca-ISE monitoring, potentiometric titration, electrokinetic measurements and surface complexation modeling. Adsorption 27, 105-115.

Tertre, E., Beaucaire, C., Coreau, N., Juery, A., 2009. Modelling Zn(II) sorption onto clayey sediments using a multi-site ion-exchange model. Appl. Geochem. 24, 1852-1861.

Thoenen, T., Hummel, W., Berner, U., Curti, E., 2014. The PSI/Nagra Chemical Thermodynamic Database 12/07, PSI report 14-04. Paul Scherrer Institut (PSI), Villigen, Switzerland.

Tournassat, C., Grangeon, S., Leroy, P., Giffaut, E., 2013. Modeling specific pH dependent sorption of divalent metals on montmorillonite surfaces. A review of pitfalls, recent achievements and current challenges. Am. J. Sci. 313, 395-451.

Tournassat, C., Tinnacher, R.M., Grangeon, S., Davis, J.A., 2018. Modeling uranium(VI) adsorption onto montmorillonite under varying carbonate concentrations: A surface complexation model accounting for the spillover effect on surface potential. Geochim. Cosmochim. Acta 220, 291-308.

Tran, E.L., Teutsch, N., Klein-BenDavid, O., Weisbrod, N., 2018. Uranium and Cesium sorption to bentonite colloids under carbonate-rich environments: Implications for radionuclide transport. Sci. Total Environ. 643, 260-269.

Van Olphen, H., 1966. An Introduction to Clay Colloid Chemistry: For Clay Technologists, Geologists, and Soil Scientists. Interscience Publ.

Vinsot, A., Mettler, S., Wechner, S., 2008. In situ characterization of the Callovo-Oxfordian pore water composition. Phys. Chem. Earth 33, S75-S86.

Vuceta, J., 1976. Adsorption of Pb(II) and Cu(II) on α-quartz from aqueous solutions: influence of pH, ionic strength, and complexing ligands. PhD thesis, California Institute of Technology, USA.

Wang, Z., Zachara, J.M., Liu, C., Gassman, P.L., Felmy, A.R., Clark, S.B., 2008. A cryogenic fluorescence spectroscopic study of uranyl carbonate, phosphate and oxyhydroxide minerals. Radiochim. Acta 96, 591-598.

Wang, Z.M., Zachara, J.M., Yantasee, W., Gassman, P.L., Liu, C.X., Joly, A.G., 2004. Cryogenic laser induced fluorescence characterization of U(VI) in Hanford vadose zone pore waters. Environ. Sci. Technol. 38, 5591-5597.

Wolter, J.-M., Schmeide, K., Weiss, S., Bok, F., Brendler, V., Stumpf, T., 2019a. Stability of U(VI) doped calcium silicate hydrate gel in repository-relevant brines studied by leaching experiments and spectroscopy. Chemosphere 218, 241-251.

Wolter, J.M., Schmeide, K., Huittinen, N., Stumpf, T., 2019b. Cm(III) retention by calcium silicate hydrate (C-S-H) gel and secondary alteration phases in carbonate solutions with high ionic strength: A site-selective TRLFS study. Sci. Rep. 9, 14255.

Xiong, Q.R., Joseph, C., Schmeide, K., Jivkov, A.P., 2015. Measurement and modelling of reactive transport in geological barriers for nuclear waste containment. Phys. Chem. Chem. Phys. 17, 30577-30589.

Zheng, Z.P., Tokunaga, T.K., Wan, J.M., 2003. Influence of calcium carbonate on U(VI) sorption to soils. Environ. Sci. Technol. 37, 5603-5608.